

RECEIVED: April 22, 2025 REVISED: June 7, 2025 ACCEPTED: June 24, 2025 PUBLISHED: July 16, 2025

Probing long-range forces in neutrino oscillations at the ESSnuSB experiment



The ESSnuSB collaboration

M. Ghosh, A. Giarnetti, A. Gupta, D. Meloni et al.

Full author list at the end of the paper

E-mail: mghosh@irb.hr, alessio.giarnetti@uniroma3.it, aman.gupta@saha.ac.in, davide.meloni@uniroma3.it

ABSTRACT: Neutrino oscillations constitute an excellent tool to probe physics beyond the Standard Model. In this paper, we investigate the potential of the ESSnuSB experiment to constrain the effects of flavour-dependent long-range forces (LRFs) in neutrino oscillations, which may arise due to the extension of the Standard Model gauge group by introducing new U(1) symmetries. Focusing on three specific U(1) symmetries — $L_e - L_\mu$, $L_e - L_\tau$, and $L_\mu - L_\tau$, we demonstrate that ESSnuSB offers a favourable environment to search for LRF effects. Our analyses reveal that ESSnuSB can set 90% confidence level bounds of $V_{e\mu} < 2.99 \times 10^{-14} \,\mathrm{eV}$, $V_{e\tau} < 2.05 \times 10^{-14} \,\mathrm{eV}$, and $V_{\mu\tau} < 1.81 \times 10^{-14} \,\mathrm{eV}$, which are competitive to the upcoming Deep Underground Neutrino Experiment (DUNE). It is also observed that reducing the systematic uncertainties from 5% to 2% improves the ESSnuSB limits on $V_{\alpha\beta}$. Interestingly, we find limited correlations between LRF parameters and the less constrained lepton mixing parameters θ_{23} and δ_{CP} , preserving the robustness of ESSnuSB's sensitivity to CP violation. Even under extreme LRF potentials $(V_{\alpha\beta} \gg 10^{-13} \,\text{eV})$, the CP-violation sensitivity and $\delta_{\rm CP}$ precision remain largely unaffected. These results establish ESSnuSB as a competitive experimental setup for probing LRF effects, complementing constraints from other neutrino sources and offering critical insights into the physics of long-range forces.

KEYWORDS: Neutrino Interactions, Non-Standard Neutrino Properties, Neutrino Mixing

ARXIV EPRINT: 2504.10480

\mathbf{C}	ontents	
1	Introduction	1
2	Theoretical formalism	3
	2.1 Long-range forces from new $U(1)$ symmetries	3
	2.2 Modified Hamiltonian due to long-range interaction potential	4
3	Simulation details of the ESSnuSB experiment	5
4	Investigating LRFs at probability and event levels	6
1 2 3 4 5 6 7 8 A	4.1 The $\nu_{\mu} \rightarrow \nu_{e}$ and $\nu_{\mu} \rightarrow \nu_{\mu}$ oscillation probabilities	7
	4.2 Event rates in the presence of LRFs	7
5	Constraint plots for ESSnuSB	9
	5.1 Correlations	12
6	CPV sensitivity of ESSnuSB in the presence of LRFs	15
7	CP precision of ESSnuSB in the presence of LRFs	17
8	Summary and conclusions	19
A	LRF induced by other $U(1)$ symmetries	20
\mathbf{T}	heoretical formalism 3 1 Long-range forces from new U(1) symmetries 3 2 Modified Hamiltonian due to long-range interaction potential 4 imulation details of the ESSnuSB experiment 5 investigating LRFs at probability and event levels 6 1 The $\nu_{\mu} \rightarrow \nu_{e}$ and $\nu_{\mu} \rightarrow \nu_{\mu}$ oscillation probabilities 7 2 Event rates in the presence of LRFs 7 onstraint plots for ESSnuSB 9 1 Correlations 12 PV sensitivity of ESSnuSB in the presence of LRFs 15 P precision of ESSnuSB in the presence of LRFs 17 ummary and conclusions 19	

1 Introduction

The discovery of neutrino oscillations [1–4] has provided compelling evidence for physics beyond the Standard Model (SM), opening new avenues to explore new fundamental interactions and forces. The unique properties of neutrinos, including their elusive nature and tiny masses, make them an excellent probe to detect even the most subtle signatures of new physics. The neutrino experiments with their increasing precision are now sensitive to sub-leading effects due to potential non-standard interactions (NSIs), offering an indirect hint of new particles and forces not predicted by the SM.

In the standard scenario, the interaction of neutrinos with matter is described by the so-called Mikheyev-Smirnov-Wolfenstein (MSW) mechanism, which results from coherent forward scattering of neutrinos with ambient matter [5]. In this seminal paper, Wolfenstein also proposed the possibility of NSIs,¹ which have been extensively studied in the literature [11–16].

¹In this manuscript, we will focus on new interactions mediated by vector bosons. There exists other forms of such interactions with different Lorentz structures [6–10], which physics signatures are however different from the ones discussed here.

In this work, we focus on another kind of such a new leptonic neutrino-matter interaction known as the long-range force (LRF), which may be flavour-dependent and mediated by light vector mediators [17–21]. This is particularly intriguing since their effects can accumulate over astronomical distances, making them distinct from other NSIs. For instance, the matter content within astrophysical objects (Sun, Earth, Milky Way, etc.) can act as a source of LRF potential. These interactions significantly modify the probabilities of neutrino oscillations by introducing new potential terms in the Hamiltonian for neutrino propagation [22]. Such interactions originate by extending the SM gauge group with additional anomaly-free U(1) symmetries associated with lepton numbers L_e, L_μ, L_τ and the baryon number B. We consider the three possible combinations of lepton flavours of symmetries [23–26], for example, $L_e - L_\mu$, $L_e - L_{\tau}$, $L_{\mu} - L_{\tau}$. These symmetries are also important for generating neutrino masses [27– 29]. The constraints on the LRF parameters have already been obtained from solar [30–32], atmospheric [33] and astrophysical neutrinos [34, 35].² In ref. [36], a global analysis of threeflavour oscillation data has been performed in the presence of flavour-dependent long-range interactions. Furthermore, the effect of LRFs on long-baseline (LBL) neutrino experiments has been explored in refs. [37–40].

A key objective of present and future neutrino oscillation experiments [41–44] is the precise determination of the leptonic CP-violating phase $\delta_{\rm CP}$. The European Spallation Source (ESS) neutrino Super-Beam ESSnuSB [45] is a next-to-next-generation long-baseline neutrino oscillation experiment designed to achieve this goal. Located in Sweden, ESSnuSB will produce a high-intensity muon neutrino beam using a 5 MW proton beam from the upgraded ESS facility in Lund [46, 47]. The neutrinos will be detected by a water-Cherenkov detector situated 360 km away from Lund at the mine in Zinkgruvan. By focusing on the second oscillation maximum in the appearance probability $P_{\mu e}$, ESSnuSB is uniquely positioned to provide a precise measurement of $\delta_{\rm CP}$. Currently, ESSnuSB is at the stage of preparation of a second conceptual design report to be followed by the development of a technical design report. This will help to plan the construction and data collection at a later stage [48, 49]. In the present work, we perform the first comprehensive study of the impact of long-range forces on the physics sensitivities of the ESSnuSB experiment. We derive bounds on the LRF potentials and the associated coupling parameters, comparing them with those achievable in the next-generation LBL experiments DUNE and T2HK. In addition, we investigate the effects of LRFs on the measurement of $\delta_{\rm CP}$ by ESSnuSB. Our analysis demonstrates that ESSnuSB's long baseline and high precision make it an ideal facility for probing the subtle effects of LRFs, offering sensitivity that surpasses those of some existing experiments.

This paper is organized as follows. In section 2, we provide a brief overview of the theoretical framework of LRFs in neutrino oscillations, focusing on the three U(1) symmetries under consideration. Then, in section 3, the description of the ESSnuSB experiment and other simulation details are provided. Next, in section 4, we compute the transition probabilities

 $^{^2}$ Most works on LRFs in neutrino oscillations take into account specific models or mediator mass ranges. The only model-independent constraints on the LRF potentials from existing experiments come from high-energetic neutrinos observed at IceCube [35] and of $\mathcal{O}(10^{-19} \text{ eV})$. These bounds are much tighter than the ones expected at terrestrial experiments due to energy-enhanced effects of LRFs. However, it is still worth exploring the bounds of accelerator experiments that employ a well-known and controlled neutrino beam.

and generate the event plots in the presence of LRFs for ESSnuSB. In section 5, the sensitivity of the ESSnuSB experiment to constrain the LRF potentials and new coupling parameters are presented. Especially, subsection 5.1 deals with some interesting correlations of LRF potentials with θ_{23} and δ_{CP} . Furthermore, in section 6, the impact of LRFs on the measurement of δ_{CP} is discussed, which is followed by a precision study of CP violation (CPV) in section 7. Finally, in section 8, we summarize our findings and conclusions.

2 Theoretical formalism

Neutrino flavour transitions are significantly influenced by the interactions between neutrinos and the ambient matter as they propagate from the source to the detector. These interactions induce an effective potential in the Hamiltonian interaction [5]. In standard scenario, neutrino-matter interactions occur through Charged Current (CC) and Neutral Current (NC) mechanisms. While standard NC interactions are flavour-universal and do not impact neutrino oscillations, possible Beyond Standard Model (BSM) neutrino-matter interactions could introduce new potential terms that significantly alter neutrino propagation. Long-range forces are one such case, which may affect the measurements of neutrino oscillations in long-baseline experiments.

2.1 Long-range forces from new U(1) symmetries

This can be envisaged by the extension of the SM gauge group $SU(3)_C \times SU(2)_L \times U(1)_Y$ with the minimal particle content by introducing the anomaly-free combination of the U(1) symmetries L_e, L_μ, L_τ and B associated with the corresponding lepton numbers and baryon numbers. There are three possible lepton flavour combinations, for instance, $L_e - L_\mu, L_e - L_\tau$, $L_\mu - L_\tau$, which can be gauged anomaly-free with the particles already present in the SM.³ In principle, these extra symmetries cannot reproduce the neutrino observables [51, 52]; however, with the addition of Higgs-like particles [27–29], neutrino mixing and mass prediction can be reconciled. In addition, they induce a new flavour-dependent neutrino-matter interactions mediated by a new neutral gauge boson Z', and if the mediator is extremely light, the resulting forces might become significant over very large distances. The magnitude of the LRFs depends upon the matter contained within the radius $R_m \sim 1/m_{Z'}$ which acts as a source of new potential.

The Lagrangian corresponding to the new interactions between a neutrino field ν_{α} and a charged lepton field l_{α} mediated by a new gauge boson Z', for the combination of U(1) symmetry $L_{\alpha} - L_{\beta}$, is given by

$$\mathcal{L}_{Z'} = g'_{\alpha\beta} Z'_{\rho} \left(\bar{l}_{\alpha} \gamma^{\rho} l_{\alpha} - \bar{l}_{\beta} \gamma^{\rho} l\beta + \bar{\nu}_{\alpha} \gamma^{\rho} P_{L} \nu_{\alpha} - \bar{\nu}_{\beta} \gamma^{\rho} P_{L} \nu_{\beta} \right), \tag{2.1}$$

where $g'_{\alpha\beta}$ denote the dimensionless new gauge couplings and P_L is the left-handed projection operator. It is to be noted that the (radiative) mixing [53, 54] between Z and Z' can also induce such long-range interactions, whose strengths are proportional to the couplings $g'_{\alpha\beta}(\xi - \sin \theta_w \chi)$ [53], where the quantity χ is the kinetic mixing parameter between Z and

³In addition to these combinations, LRFs can also arise from other new U(1) symmetries, as discussed in ref. [50]. The corresponding ESSnuSB constraints on certain textures are provided in appendix A.

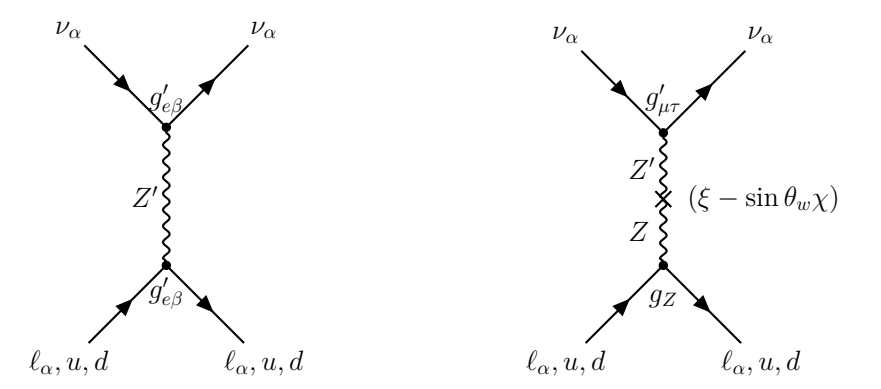


Figure 1. Feynman diagrams of the new neutrino-matter interactions mediated by the new Z' neutral vector boson. The left diagram represents the interaction in the $L_e - L_\beta$ case, while the right diagram represents the interaction contributing to neutrino oscillations in the $L_\mu - L_\tau$ case, where the mixing between the Z boson and the new Z' is needed. Here, g_Z refers to the usual Z boson coupling with leptons and quarks.

Z' [53, 55], the quantity ξ is the rotation angle between mass and flavour bases of the gauge bosons and θ_w is the Weinberg angle. In figure 1, we show the NC-like neutrino interactions mediated by Z' boson which can modify the oscillation probabilities; the left (right) diagram refers to the $L_e - L_\beta$ ($L_\mu - L_\tau$) case, see the following section for details.

2.2 Modified Hamiltonian due to long-range interaction potential

Assuming the three new U(1) gauge symmetries $L_e - L_{\mu}$, $L_e - L_{\tau}$ and $L_{\mu} - L_{\tau}$ that induce new neutrino-matter interactions, the effective Hamiltonian for neutrino propagation in the flavour basis is

$$H^{\text{eff}} = \frac{1}{2E} \left[U \begin{pmatrix} 0 & 0 & 0 \\ 0 & \Delta m_{21}^2 & 0 \\ 0 & 0 & \Delta m_{31}^2 \end{pmatrix} U^{\dagger} \right] \pm V_{\text{CC}} \begin{pmatrix} 1 & 0 & 0 \\ 0 & 0 & 0 \\ 0 & 0 & 0 \end{pmatrix} \pm V_{\alpha\beta}. \tag{2.2}$$

In the above expression, U is the standard Pontecorvo-Maki-Nakagawa-Sakata (PMNS) mixing matrix in vacuum, and $V_{\rm CC} = \sqrt{2}G_F N_e$ is the usual matter potential term due to the CC interactions of neutrinos with matter.⁴ The signs of $V_{\rm CC}$ and $V_{\alpha\beta}$ are positive (negative) in the case of neutrino (antineutrino) oscillations. The neutrino energy is denoted by E, and N_e is the electron number density. The contribution due to the long-range interaction is given by the new potential $V_{\alpha\beta}$ which, for the three different symmetries, can be written as

$$V_{\alpha\beta} = \begin{cases} \operatorname{diag}(V_{e\mu}, -V_{e\mu}, 0), & \text{for } L_e - L_{\mu} \\ \operatorname{diag}(V_{e\tau}, 0, -V_{e\tau}), & \text{for } L_e - L_{\tau} \\ \operatorname{diag}(0, V_{\mu\tau}, -V_{\mu\tau}), & \text{for } L_{\mu} - L_{\tau} \end{cases}$$
 (2.3)

The specific form of the LRF Lagrangian generates a Yukawa-like potential with an interaction length inversely proportional to the mediator mass [34, 64]. Under transformations of the

⁴NC interactions in neutrino propagation do not contribute to the oscillation probabilities in the usual three active neutrino framework. It is worth to mention that, in presence of sterile neutrinos or other forms of new physics, they could affect the matter-induced modifications of the vacuum neutrino oscillation probabilities [56–63].

symmetry $L_e - L_\beta$, where $\beta = \mu, \tau$, this potential will be sourced by a population of electrons N_e located at a distance d from the neutrinos on Earth and is given as [34, 39]

$$V_{e\beta} = G_{e\beta}^2 \frac{N_e}{4\pi d} e^{-m_{Z'}d}, \qquad (2.4)$$

where $G_{e\beta}$ is the effective coupling (which corresponds to $g'_{e\beta}$ in eq. (2.1), $m_{Z'}$ is the mass of new mediating gauge boson Z'. For $L_{\mu} - L_{\tau}$, the LRF is originated from the mixing between new gauge boson Z' and the SM gauge boson Z [54, 65]. In this case, assuming the Universe to be electrically neutral, the new potential experienced by neutrinos is only due to its interaction with N_n number of neutrons which is given by [65]

$$V_{\mu\tau} = G_{\mu\tau}^2 \frac{e}{\sin \theta_w \cos \theta_w} \frac{N_n}{4\pi d} e^{-m_{Z'}d},$$
 (2.5)

where e is the electric charge. For the $L_{\mu} - L_{\tau}$ symmetry, the effective coupling $G_{\mu\tau}$ is related to the coupling $g'_{\mu\tau}$ as $G_{\mu\tau} = \sqrt{g'_{\mu\tau}(\xi - \sin\theta_w \chi)}$ [53].

It is worth mentioning that the structure of the new interaction potential is very similar to the standard matter potential except for the fact that in the former case, the mediator is extremely light (Z'), while in the latter case, the mediator is very heavy (the SM Z boson). For this reason, LRFs can introduce new resonances in the transition probabilities at lower energies than the usual MSW resonance [5] such as [37, 38]

$$E_{\rm res} = \frac{\Delta m_{31}^2 \cos 2\theta_{13}}{2V_{\rm CC} + 3V_{e\beta}},\tag{2.6}$$

for the L_e-L_β case. No resonances are expected in the $L_\mu-L_\tau$ scenario [50, 66]. However, deriving expressions for neutrino oscillation probabilities in the presence of LRFs is cumbersome and not very enlightening. In some works, the "effective" mixing angles and mass-squared differences are computed using particular approximations and assumptions [37, 39, 40]. It should be noted that, at the Hamiltonian level, the effect of long-range forces is the same as the effect of flavour conserving vector NSIs [40, 62, 64, 66]. As it can be noted from analytical expansions presented in refs. [6, 67], the flavour conserving vector NSI parameters appear in the oscillation probabilities as sub-leading effects in the $\nu_\mu \to \nu_e$ channel and at the first order in the $\nu_\mu \to \nu_\mu$ channel. However, given the presence of the new resonance in eq. (2.6) in the ν_e appearance probability and since to be sensitive to LRF parameters we need $V_{\alpha\beta}$ of the order of the standard matter effect, the overall effects of LRFs cannot be fully understood from analytical expansions in small new physics parameters. In this work, we discuss the LRF effects on the probabilities only numerically in section 4.1.

3 Simulation details of the ESSnuSB experiment

To generate the probability spectrum, analyze event rates, and perform sensitivity studies of ESSnuSB in the presence of LRFs, we employed the GLoBES software [68, 69]. We introduced modifications to the probability engine to incorporate new potential terms due to the LRF as a new physics effect and then carried out numerical computations to obtain event rates and χ^2 values. The experimental configuration and parameters for ESSnuSB used

Oscillation parameters (3ν)	Normal ordering (NO)
$ heta_{12}(^{\circ})$	$33.41^{+0.75}_{-0.72}$
$\theta_{23}(^{\circ})$	$42.2_{-0.9}^{+1.1}$
θ ₁₃ (°)	$8.58^{+0.11}_{-0.11}$
$\delta_{\mathrm{CP}}(^{\circ})$	232^{+36}_{-26}
$\Delta m_{21}^2 \ (\text{eV}^2)$	$7.41^{+0.21}_{-0.20} \times 10^{-5}$
$\Delta m_{31}^2 \; (\text{eV}^2)$	$+2.507^{+0.026}_{-0.027} \times 10^{-3}$

Table 1. The best-fit value of the neutrino oscillation parameters in the standard three-flavour framework assuming normal mass ordering of neutrinos (NO). The values and their 1σ uncertainty intervals used in our calculations are taken from ref. [71], which is the NuFit 5.2 data presented in 2022.

in our study are based on the ESSnuSB Conceptual Design Report [47] and were therefore implemented in GLoBES.

In particular, we considered a water Cherenkov far detector with a fiducial volume of 538 kt, positioned in the mine at Zinkgruvan, 360 km away from the neutrino source at ESS in Lund. A powerful linear accelerator (linac) will deliver 2.7×10^{23} protons on target per year, with a beam power of 5 MW and a proton kinetic energy of 2.5 GeV. We adopted updated neutrino fluxes, peaking at approximately 0.25 GeV, and applied updated migration matrices for event selection, as outlined in refs. [47, 70]. The energy spectrum in the [0, 2.5] GeV range was divided into 50 bins for event calculations.

Our analyses included both the appearance $(\nu_{\mu} \to \nu_{e})$ and disappearance $(\nu_{\mu} \to \nu_{\mu})$ channels and their CP-conjugate transitions, and accounted for all the relevant backgrounds. We assumed systematic errors of 5% for signals and 10% for backgrounds unless otherwise stated. The total exposure time assumed for the far detector is 10 years, equally divided between 5 years of running the neutrino beam and 5 years for the antineutrino beam.

4 Investigating LRFs at probability and event levels

In this section, we first examine how the appearance and disappearance oscillations probabilities of muon neutrinos are influenced by the presence of a new interaction potential, $V_{\alpha\beta}$, sourcing the LRF at the ESSnuSB energies. Subsequently, we analyze the expected total event rates under the inclusion of LRFs in the theoretical framework. Unless stated otherwise, we adopt the best-fit values for the standard oscillation parameters from NuFIT 5.2 [71, 72], which incorporate Super-Kamiokande atmospheric data and these parameters are summarized in table 1. For this analysis, we focus solely on the normal mass ordering (NO) for neutrinos, in line with the global fit preference for NO [73–77], which might also be suggested by recent DESI-BAO cosmological results [78].

4.1 The $\nu_{\mu} \rightarrow \nu_{e}$ and $\nu_{\mu} \rightarrow \nu_{\mu}$ oscillation probabilities

In figure 2, we display the plots for neutrino oscillation probabilities, computed numerically in the presence of LRF potentials, $V_{\alpha\beta}$, as a function of neutrino energy relevant for the ESSnuSB experiment. To show the impact of LRF potentials, we set their values, $V_{\alpha\beta} = 1.3 \times 10^{-13} \,\text{eV}$, which is of the same order of magnitude as the standard matter potential [39, 62]. The top (bottom) panel is presented for the neutrino (antineutrino) oscillation probability. The left (right) panel depicts the effect of $V_{\alpha\beta}$ on the appearance (disappearance) channel. In each panel, the solid curves denote the standard probabilities without $V_{\alpha\beta}$, while the dashed, dotted and dash-dotted curves refer to potentials, $V_{\alpha\beta}$, corresponding to the three different symmetries, $L_e - L_{\mu}$, $L_e - L_{\tau}$ and $L_{\mu} - L_{\tau}$, respectively. Moreover, two extreme values for δ_{CP} have been chosen, corresponding to the case of maximal CP violation ($\delta_{\text{CP}} = -90^{\circ}$, black curve) and vanishing CP violation ($\delta_{\text{CP}} = 0^{\circ}$, red curve). To show the energy region relevant for the ESSnuSB experiment in each figure, we also superimpose the ESSnuSB flux multiplied by the charged current (CC) neutrino cross-section.

From figure 2 (top left), we observe that the neutrino appearance probability, $P_{\mu e}$, is enhanced around the first oscillation maximum in all three cases due to the presence of LRF potentials, whereas for antineutrino case, the appearance probability (bottom left), $\bar{P}_{\mu e}$, is suppressed. This is because the sign of LRF potential is flipped $(V_{\alpha\beta} \to -V_{\alpha\beta})$ for the antineutrino case, similar to the standard matter potential. However, around the second oscillation maximum, the appearance probability increases for both the neutrino and antineutrino cases. For the neutrino appearance probability, $P_{\mu e}$, the first oscillation maximum also shifts towards lower energies for all three cases of LRF potentials, $V_{\alpha\beta}$. We also notice that the effects are more significant for the LRF potential $V_{e\tau}$ (dotted curve), whereas $V_{e\mu}$ (dashed curve) affects mildly. The disappearance channel, on the other hand, is less affected by $V_{\alpha\beta}$ compared to the appearance one for all three cases. In particular, at the first oscillation minimum, the effect of $V_{e\mu}$ is larger for neutrinos (top right), while for antineutrinos (bottom right), the effect is more visible for $\mu\tau$ and $e\tau$ cases. However, given the much larger expected ν_{μ} number of events at the far detector, the small disappearance probability modifications due to LRFs are crucial in constraining LRF potentials, $V_{\alpha\beta}$.

4.2 Event rates in the presence of LRFs

In order to make an initial guess about the limits that ESSnuSB would set on LRF parameters, $V_{\alpha\beta}$, we plot the total number of neutrino appearance (and disappearance) events as a function of the LRF parameter for 10 years of running, 5 in neutrino and 5 in antineutrino mode. The potential, $V_{\alpha\beta}$, is varied from $10^{-15}\,\mathrm{eV}$ to $10^{-12}\,\mathrm{eV}$. The results are presented in figure 3, where the left panel is for the appearance of electron neutrino events and the right one refers to events corresponding to the disappearance of muon neutrinos. The black curves in each plot depict the case of maximal CP violation ($\delta_{\mathrm{CP}} = -90^{\circ}$), while red curves refer to the case of CP conservation ($\delta_{\mathrm{CP}} = 0^{\circ}$). The features observed in the discussion of the probabilities can be directly translated into these plots. Indeed, in each case, we can observe a transition from the standard case (without LRFs) to the LRF-dominated case. The transition begins for values of LRF potentials, $V_{\alpha\beta}$, for which the correction in the standard probability due to the presence of LRFs overcomes the standard matter probability. A rough estimate

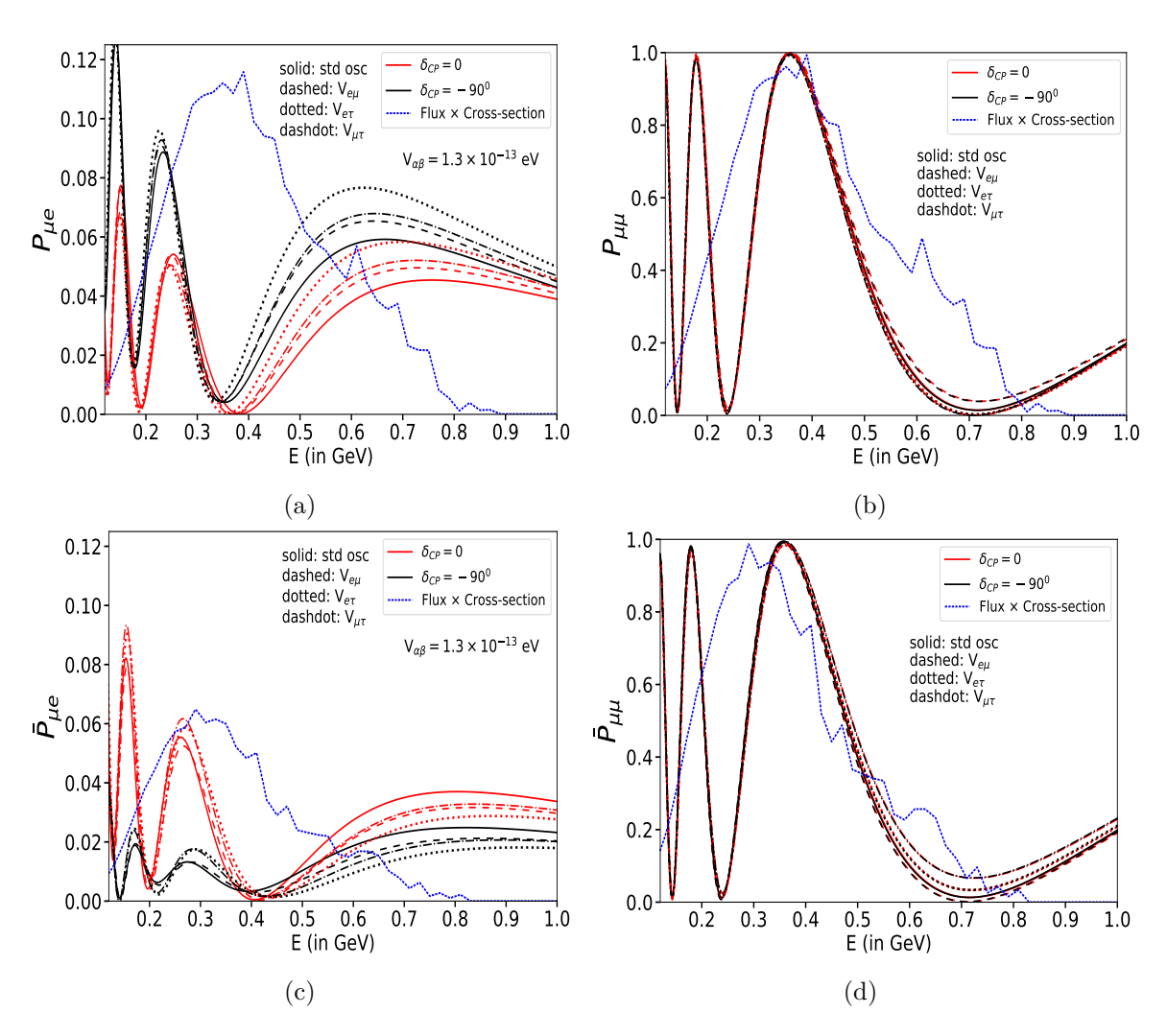


Figure 2. Appearance (left panel) and disappearance (right panel) neutrino (top panel) and antineutrino (bottom panel) oscillation probabilities as functions of neutrino energy in the presence of LRF potentials, $V_{\alpha\beta}=1.3\times 10^{-13}\,\mathrm{eV}$. The dashed, dotted and dashdot curves refer to the L_e-L_μ , L_e-L_τ and $L_\mu-L_\tau$ cases, respectively. The blue curve in each plot represents the flux × cross-section in the regions relevant for the ESSnuSB experiment.

of the constraint on $V_{\alpha\beta}$ that is obtainable from the ESSnuSB experiment can be derived directly from figure 3, $V_{\alpha\beta} \ll 10^{-13} \, \mathrm{eV}$; indeed, for larger potentials the expected number of events is much larger than the one expected in the case $V_{\alpha\beta} \to 0$. However, the detailed χ^2 analysis illustrated in the following section reveals stronger and more precise bounds on the LRF potentials. It can be observed from figure 3 that for $V_{e\tau}$ in the appearance case and $V_{e\mu}$ in the disappearance one, the number of events increases for both values of δ_{CP} . The ν_{μ} disappearance events, however, decrease in the range $10^{-14}-10^{-13}\,\mathrm{eV}$, with $V_{\alpha\beta}$ under transformations of the L_e-L_{τ} and $L_{\mu}-L_{\tau}$ symmetries.

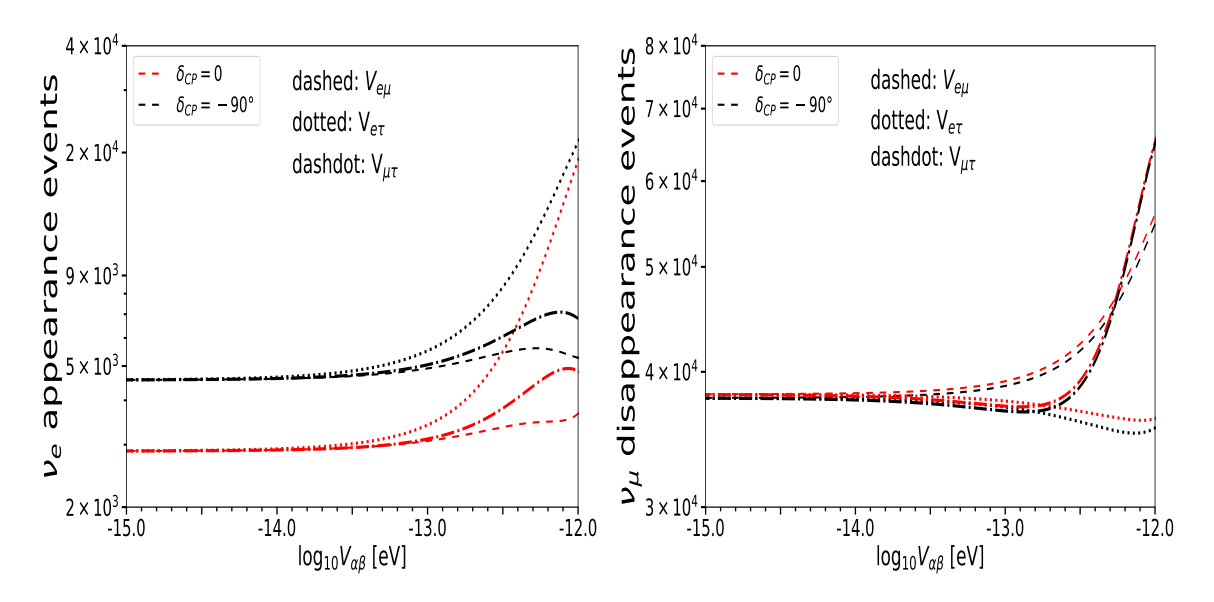


Figure 3. Total expected number of events is plotted as a function of LRF potential for the ESSnuSB experiment for two choices of $\delta_{\rm CP} = 0$ and -90° . Appearance events are shown in the left panel and disappearance events in the right panel.

5 Constraint plots for ESSnuSB

In this section, we explore the capability of the ESS nuSB experiment to constrain the parameters of LRFs. The statistical analysis has been performed using a Poissonian χ^2 function, defined as

$$\chi^{2}(\vec{\Lambda}, b) = 2\sum_{i=1}^{n} \left[(1+b)E_{i} - O_{i} + O_{i} \log \frac{O_{i}}{(1+b)E_{i}} \right] + \frac{b^{2}}{\sigma_{b}^{2}},$$
 (5.1)

where $\vec{\Lambda}$ represents the set of oscillation parameters needed to compute the rates, σ_b is the normalization error, n is the number of energy bins, O_i are the observed rates and E_i are the expected rates used for the fit. Systematic uncertainties are incorporated using the *pull method* [79, 80], implemented in GLoBES with the nuisance parameter b. The significance of our results in terms of standard deviations (σ) has been obtained assuming the Wilk's theorem [81]; for instance, for 1 d.o.f $\#\sigma = \sqrt{\Delta \chi^2}$.

In order to compute the bounds on $V_{\alpha\beta}$, we generate the true event spectrum using the hypothesis of no LRFs (i.e. $V_{\alpha\beta}$ (true) = 0) corresponding to standard three-flavour neutrino oscillations and fit the true data using the probabilities in the presence of LRFs. It should be noted that, while fitting the true data, only one LRF parameter is considered at a time in the test. This approach is justified as different potentials stem from distinct symmetries, independently affecting the oscillations. In all three cases of symmetries, we vary the potentials, $V_{\alpha\beta}$ from 10^{-15} eV to 10^{-13} eV in the test. The marginalization has been performed over θ_{13} , θ_{23} and $|\Delta m_{31}^2|$ by varying them within the uncertainty ranges reported in table 1, while $\delta_{\rm CP}$ is scanned over its full $[-180^{\circ}, 180^{\circ}]$ range. We keep the two oscillation parameters, θ_{12} and Δm_{21}^2 , fixed at their best-fit values [71]. The results are displayed in figure 4 where the one-dimensional $\Delta \chi^2$ is plotted as a function of LRF potentials $V_{\alpha\beta}$. The

upper left (right) plot of figure 4 gives the bound on the LRF parameter $V_{e\mu}$ ($V_{e\tau}$) while the lower plot displays the constraint on $V_{\mu\tau}$. We also show the results for different values of the normalization systematic uncertainty, namely 2% (red curves), 5% (blue curves) and 10% (green curves). The 3σ and 90% C.L. bounds are summarized in table 2 for the standard 5% systematics case along with the 2% and 10% systematics cases. The main results are that ESSnuSB in the nominal conditions (i.e. 5% systematics) may be able to set the 90% limits on $V_{e\mu} < 2.99 \times 10^{-14} \, \text{eV}$, $V_{e\tau} < 2.05 \times 10^{-14} \, \text{eV}$ and $V_{\mu\tau} < 1.81 \times 10^{-14} \, \text{eV}$. Notably, a change between 10% and 20% in the bounds can also be observed by variations in systematic uncertainties, particularly when $V_{e\mu}$ and $V_{e\tau}$ are considered. The effect of systematics on $V_{\mu\tau}$ is, on the other hand, less prominent.

Before comparing the ESSnuSB limits on LRF potentials with other experimental bounds, let us try to understand the role of appearance and disappearance channels in constraining $V_{\alpha\beta}$. In figure 5, we demonstrate how individual probability channels contribute for the ESSnuSB sensitivity towards LRF potentials, $V_{\alpha\beta}$. It is evident that for the $L_e - L_{\mu}$ and $L_{\mu} - L_{\tau}$ symmetries the major sensitivity comes from the disappearance $(P_{\mu\mu})$ probability, whereas the appearance probability $(P_{\mu e})$ plays a major role to place a bound on the $V_{e\tau}$ potential corresponding to the $L_e - L_\tau$ symmetry. This is also clear from the probability plots presented in figure 2, where the effect of the $e\tau$ sector is more visible in the appearance probability $(P_{\mu e})$. Although from figure 2, it seems that the $e\mu$ and $\mu\tau$ sectors affect both $P_{\mu e}$ and $P_{\mu \mu}$, however, due to the high statistics of ν_{μ} the disappearance event numbers at the far detector, disappearance channel plays an important role in constraining $V_{e\mu}$ and $V_{\mu\tau}$. This explains why different oscillation channels are sensitive to different LRF potentials. In figure 5, we notice a dip corresponding to the disappearance-only sensitivity curves (blue solid curves) for all three cases of the LRF potentials when a marginalization over θ_{23} is performed. Similar features are also observed in other works [39, 40]. This is because, in the disappearance probability, the octant of θ_{23} develops a degeneracy with the potential $V_{\alpha\beta}$ picking up the wrong solution in the minimum χ^2 calculation when marginalization is performed over θ_{23} . The dip vanishes for the disappearance only case if we fix θ_{23} to its best-fit value while computing the χ^2 . Also, the dip disappears when we combine both the appearance and disappearance channels (green solid curves), while marginalizing over θ_{23} , highlighting the importance of the appearance channel, which is less affected by the θ_{23} octant degeneracy.

In the context of LBL experiments, the most stringent foreseen 90% C.L. limits on LRF potentials have been derived by simulating the future experiment P2SO [40] due to its longer baseline, whereas the bounds (at 90% C.L.) from the simulations of "upcoming" DUNE and T2HK experiments with the standard neutrino flux are given by [39]:

$$V_{e\mu} < 1.46 \ (3.45) \times 10^{-14} \text{ eV} \ [DUNE \ (T2HK)],$$

 $V_{e\tau} < 1.03 \ (3.43) \times 10^{-14} \text{ eV} \ [DUNE \ (T2HK)],$
 $V_{\mu\tau} < 0.67 \ (1.84) \times 10^{-14} \text{ eV} \ [DUNE \ (T2HK)].$ (5.2)

It is worth mentioning that with a high-energy neutrino flux, the DUNE bounds on $V_{\alpha\beta}$ might become weaker as shown in ref. [62].

Comparing the ESSnuSB results with other expected limits from upcoming LBL experiments in eq. (5.2), we find that assuming nominal conditions (5% systematics), ESS-

LRF Potential (in eV)	3σ C.L.			90% C.L.		
	2% syst.	5% syst.	10% syst.	2% syst.	5% syst.	10% syst.
$V_{e\mu}(\times 10^{-14})$	4.41	5.89	7.28	2.37	2.99	3.44
$V_{e\tau}(\times 10^{-14})$	2.86	3.79	4.68	1.57	2.05	2.54
$V_{\mu\tau}(\times 10^{-14})$	2.75	3.34	3.67	1.48	1.81	1.92

Table 2. Constraints on the LRF potential $V_{\alpha\beta}$ from the ESSnuSB experiment for 2%, 5% and 10% systematics. These values are obtained from the plots displayed in figure 4.

nuSB bounds are less stringent than the DUNE ones by about a factor of 2. This is due to the higher energy and longer baseline for DUNE, so the effect of LRFs is more pronounced. However, ESSnuSB outperforms T2HK by approximately 20%. As mentioned earlier, systematic uncertainties play a noticeable role in placing bounds on the LRF potential by ESSnuSB, i.e., achieving a 2% normalization uncertainty could improve the $V_{e\mu}$ and $V_{e\tau}$ constraints, making them comparable to future DUNE bounds. Overall, ESSnuSB is projected to set bounds on LRF parameters that are competitive with those from future LBL experiments such as DUNE and T2HK. Importantly, the complementarity of constraints from various neutrino sources, including accelerator, atmospheric, and solar neutrino data, provides a unique opportunity to significantly narrow the allowed parameter space for LRFs. By combining these results, the interplay between different datasets may uncover synergies that enhance sensitivity to LRF parameters and help elucidate the underlying physics of these new interactions.

In addition to the LRF potentials, $V_{\alpha\beta}$, we also put constraints on the actual parameters of the new neutrino-matter interaction, namely, the mass of the new gauge boson $m_{Z'}$ and the effective gauge couplings $G_{\alpha\beta}$. Following the methodology presented in refs. [34, 39, 62], we use eqs. (2.4) and (2.5) to derive the limits on $m_{Z'}$ and $G_{\alpha\beta}$. In order to take into account all the matter content present in the Universe, we consider neutrinos from different sources ranging at distances up to 10^3 Gp away from the Earth. This corresponds to the mediator mass, $m_{Z'}$ in the range $10^{-10}-10^{-35}\,\mathrm{eV}$ and the LRF potentials originating from all the matter content of the Universe can be rewritten in terms of the contributions from effective potentials relevant at different distances, i.e.,

$$V_{\alpha\beta} = (V_{\alpha\beta})_{\text{Earth}} + (V_{\alpha\beta})_{\text{Moon}} + (V_{\alpha\beta})_{\text{Sun}} + (V_{\alpha\beta})_{\text{MW}} + (V_{\alpha\beta})_{\text{Cosm}}. \tag{5.3}$$

To find the electron and neutron numbers for the LRF potentials from the Earth, an average density of a continuous distribution is modeled for the Earth such that we get $(N_e)_{\text{Earth}} = (N_n)_{\text{Earth}} \sim 4 \times 10^{51}$. The Moon and the Sun are assumed to be point-like electron and neutron sources which correspond to the number of electrons and neutrons as given by $(N_e)_{\text{Moon}} = (N_n)_{\text{Moon}} \sim 5 \times 10^{49}$ and $(N_e)_{\text{Sun}} \approx (N_n)_{\text{Sun}} \sim 10^{57}$ [39]. In case of the Milky Way, the total matter content can be assumed to be distributed in the form of a thin and a thick disk, a central bulge and a diffuse gas [34, 82, 83], yielding $(N_e)_{\text{MW}} = (N_n)_{\text{MW}} \sim 10^{67}$. For the cosmological matter content, we use $(N_e)_{\text{Cosm}} \approx (N_n)_{\text{Cosm}} \sim 10^{79}$ adopted from refs. [34, 39]. Utilizing these values of electron and neutron numbers and using eqs. (2.4) and (2.5), the contributing terms of LRF potentials from all sources can be computed provided that the values of $m_{Z'}$ and $G_{\alpha\beta}$ are known. To constrain $m_{Z'}$ and $G_{\alpha\beta}$, we use the

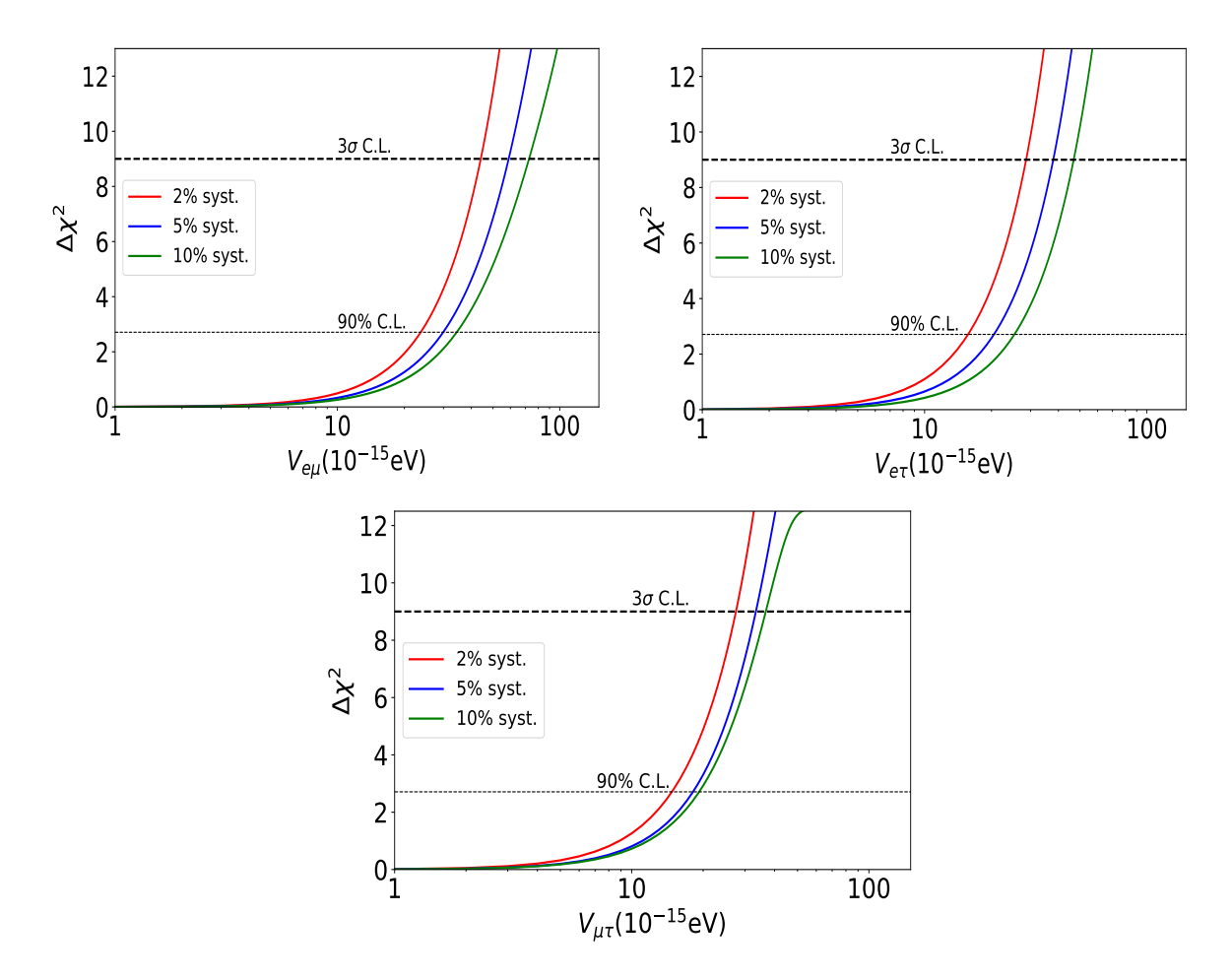


Figure 4. Sensitivity of ESSnuSB in constraining the LRF potential $V_{\alpha\beta}$. We consider normal mass ordering for neutrinos i.e., $\Delta m_{31}^2 > 0$. The red, blue and green colours correspond to the cases for 2%, 5% and 10% systematic uncertainties, respectively.

90% C.L. limits on $V_{\alpha\beta}$ obtained in table 2 and vary the free parameters. The results are presented in figure 6 where red, blue and green curves correspond to the $L_e - L_{\mu}$, $L_e - L_{\tau}$ and $L_{\mu} - L_{\tau}$ symmetries, respectively. We also show the interaction range $\propto 1/m_{Z'}$ on the upper axis of the plot. It is worthwhile to mention that some astrophysical and cosmological phenomena, such as black-hole superradiance [84] and weak gravity conjecture [85] may also exclude some parameter space of the LRFs, providing the non-oscillation exclusion limits. These regions are displayed by the grey bands in figure 6. From this figure, one can observe that the most stringent limit comes from the location of the causal horizon, which contains the highest number of electrons and neutrons. Therefore, the LRF potentials experienced by neutrinos from this location will be the largest.

5.1 Correlations

In this subsection, we want to explore the correlations between the LRF potentials, $V_{\alpha\beta}$ and the two poorly constrained standard neutrino oscillation parameters for ESSnuSB, namely $\delta_{\rm CP}$ and θ_{23} . To conduct this analysis, the true event spectra were generated under the

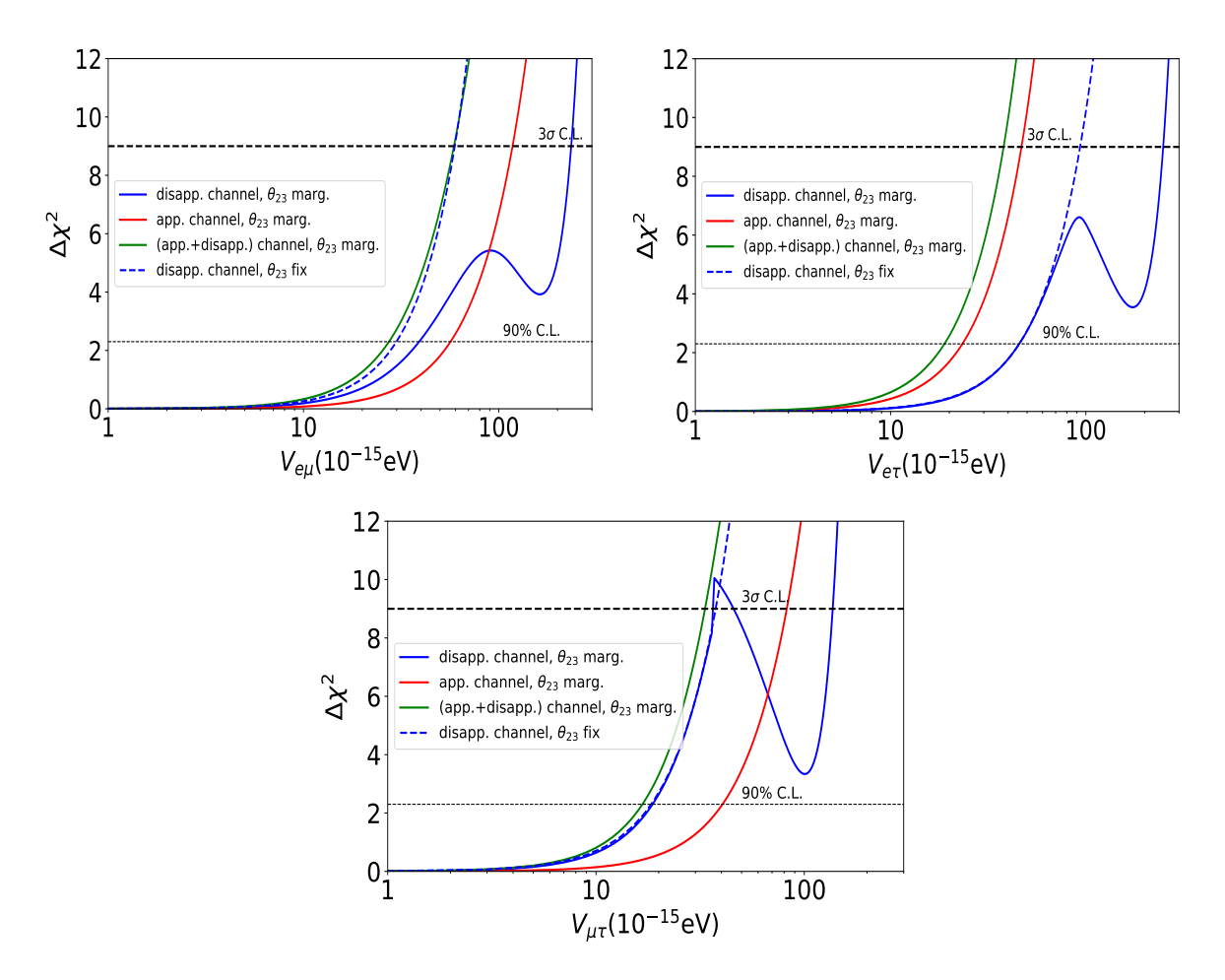


Figure 5. Significance of appearance and disappearance channels in computing the sensitivity of ESSnuSB to constrain the LRF potentials. Dashed curves show the effect of fixing θ_{23} to its best-value in the disappearance channel.

assumption of no LRFs, using the best-fit values for the standard oscillation parameters listed in table 1. The fit was obtained by marginalizing over all standard oscillation parameters not explicitly shown, except for θ_{12} and Δm_{21}^2 . Figure 7 displays the 3σ allowed regions in the $V_{\alpha\beta}-\theta_{23}$ plane. The upper-left and upper-right panels illustrate the correlations between $V_{e\mu}$ (upper left), $V_{e\tau}$ (upper right) and θ_{23} whereas the lower panels represent the correlation in the $V_{\mu\tau}-\theta_{23}$ plane. We present the results for two different choices of true values of the mixing angle θ_{23} , one in the lower octant (42.2°) and one in the upper octant (49.1°). These values correspond to the best-fits from ref. [71], with and without the inclusion of the Super-Kamiokande atmospheric data. We see that, in the absence of LRFs, the ESSnuSB results suggest that the θ_{23} octant degeneracy might not be resolved if the true value is $\theta_{23}=42.2^{\circ}$. In this case, allowed values in the upper octant persist. However, in the presence of LRFs, this degeneracy appears to be resolved as the LRF potentials $V_{e\mu}$ and $V_{e\tau}$ tend to increase (see the upper left and right panels of figure 7). A similar trend is observed for $V_{\mu\tau}$ (lower panel), although at relatively larger values of the potential. On the other hand, for $\theta_{23}=49.1^{\circ}$ and $V_{\alpha\beta}\to 0$, the octant degeneracy appears to be already broken. Even in

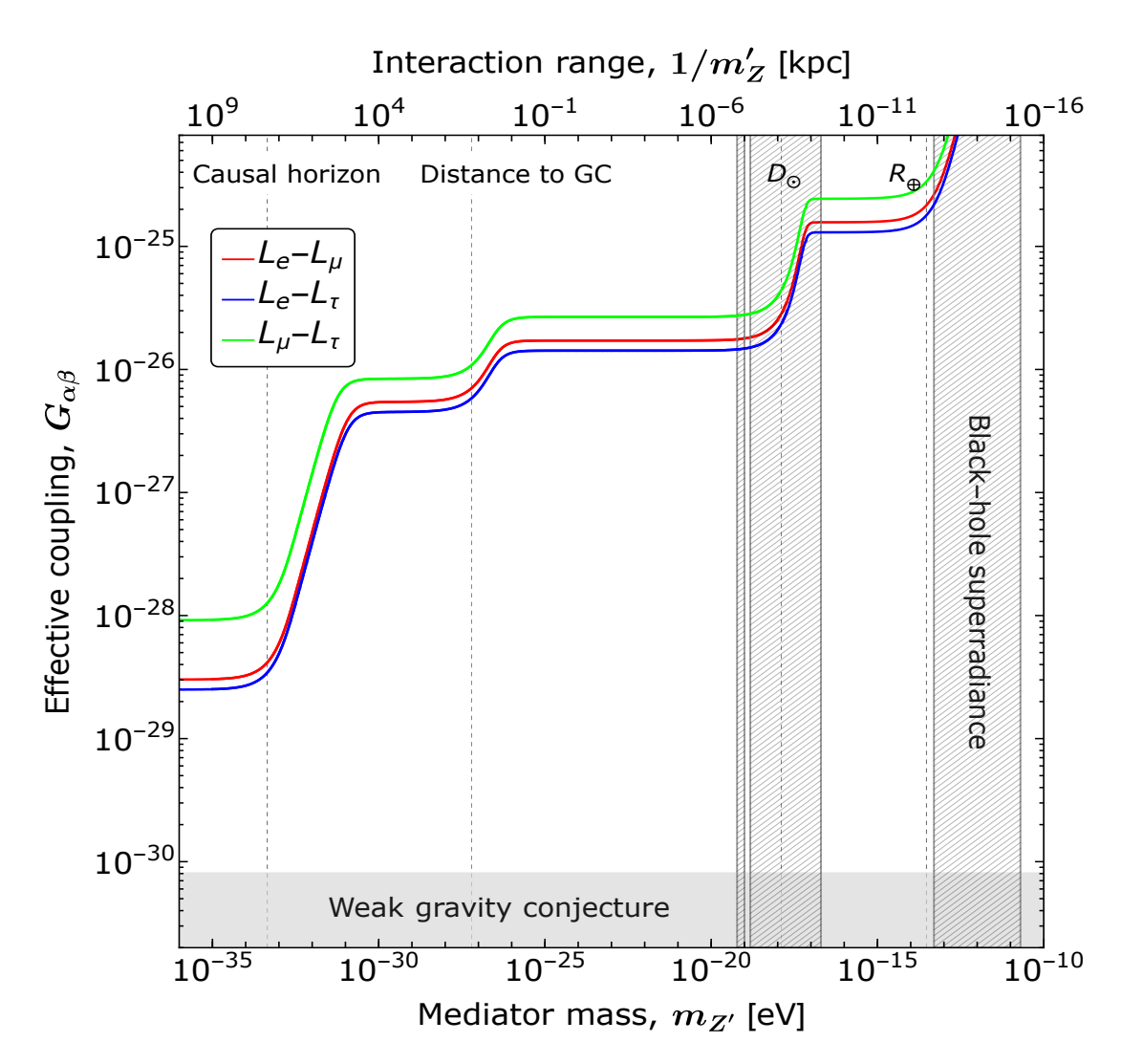


Figure 6. Sensitivity of ESSnuSB to exclude the parameter space of the LRF in the $m_{Z'} - G_{\alpha\beta}$ plane. These exclusion regions are computed at 90% C.L. by fixing the LRF potentials to their 90% C.L. values presented in table 2. See the text for more details on how the calculations were performed.

the presence of LRFs, we do not see any octant ambiguity when the true value of $\theta_{23} = 49.1^{\circ}$. As discussed in the previous section, we remark that the octant degeneracy breaking is mainly due to the appearance channel. Indeed, if we only consider the disappearance channel, the octant ambiguity plays a major role in the analysis.

In figure 8, we present the results in the $V_{e\mu} - \delta_{\rm CP}$ (upper-left panel), $V_{e\tau} - \delta_{\rm CP}$ (upper-right panel) and $V_{\mu\tau} - \delta_{\rm CP}$ (lower panel) planes for two true values of $\delta_{\rm CP}$ corresponding to maximal CPV ($\delta_{\rm CP} = -90^{\circ}$) and no CPV ($\delta_{\rm CP} = 0^{\circ}$). The marginalization scheme used in this analysis follows the same procedure as previously described, where all other oscillation parameters, except θ_{12} and Δm_{21}^2 , are marginalized. In this case, we observe no significant correlations between $\delta_{\rm CP}$ and any of the LRF potentials, $V_{e\mu}$, $V_{e\tau}$ and $V_{\mu\tau}$. However, it is worth noting that the effects of $V_{\alpha\beta}$ on the determination of $\delta_{\rm CP}$ could become significant if the LRF strengths are large enough to achieve the sensitivity of the ESSnuSB experiment. In

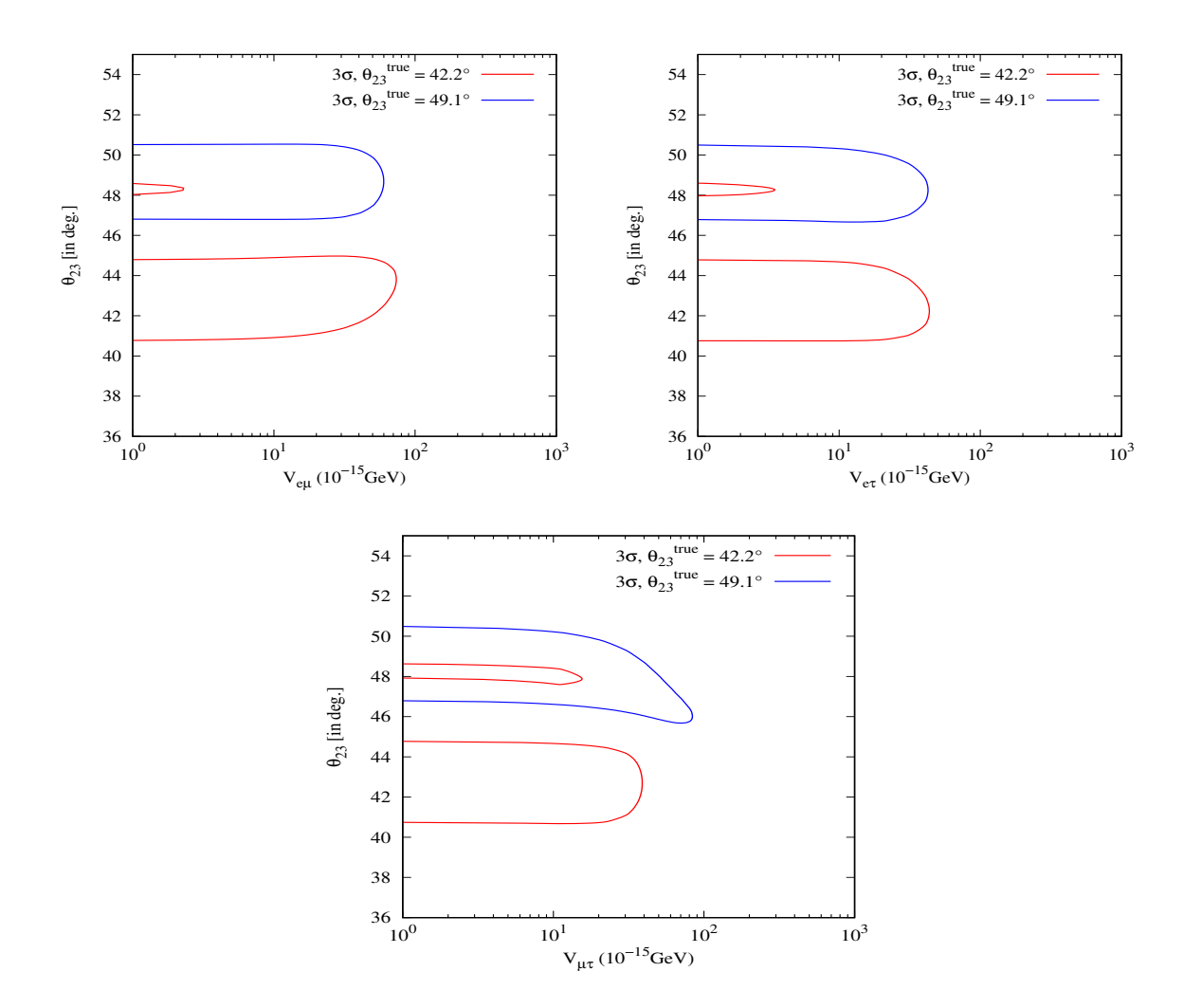


Figure 7. Effect of long-range interactions in the determination of the θ_{23} octant. In all panels, two distinct true values for the mixing angle θ_{23} have been chosen, i.e., $\theta_{23}^{\text{true}} = 42.2^{\circ}$ and 49.1° .

such a scenario, those values might become measurable, introducing a potential influence on $\delta_{\rm CP}$ determination. We will delve deeper into this possibility and its implications in the next section.

6 CPV sensitivity of ESSnuSB in the presence of LRFs

In this section, we examine how the LRF potentials influence the CP-violation sensitivity of the ESSnuSB experiment. This analysis is crucial, as the primary aim of ESSnuSB is to achieve precise measurements of $\delta_{\rm CP}$. It is worth noting that, in the case of maximal CP violation ($\delta_{\rm CP} = \pm 90^{\circ}$), the sensitivity of ESSnuSB can reach up to 12.5σ and it can also achieve at least 5σ sensitivity for approximately 75% of the other possible values of $\delta_{\rm CP}$ [9, 47]. This surpasses the sensitivity of all upcoming next-generation LBL neutrino oscillation experiments [86]. It is, therefore, vital to determine whether the presence of new physics, such as long-range interactions of neutrinos with matter, could jeopardize this capability or not. To do this, we generate the true event spectrum by varying $\delta_{\rm CP}$ (true)

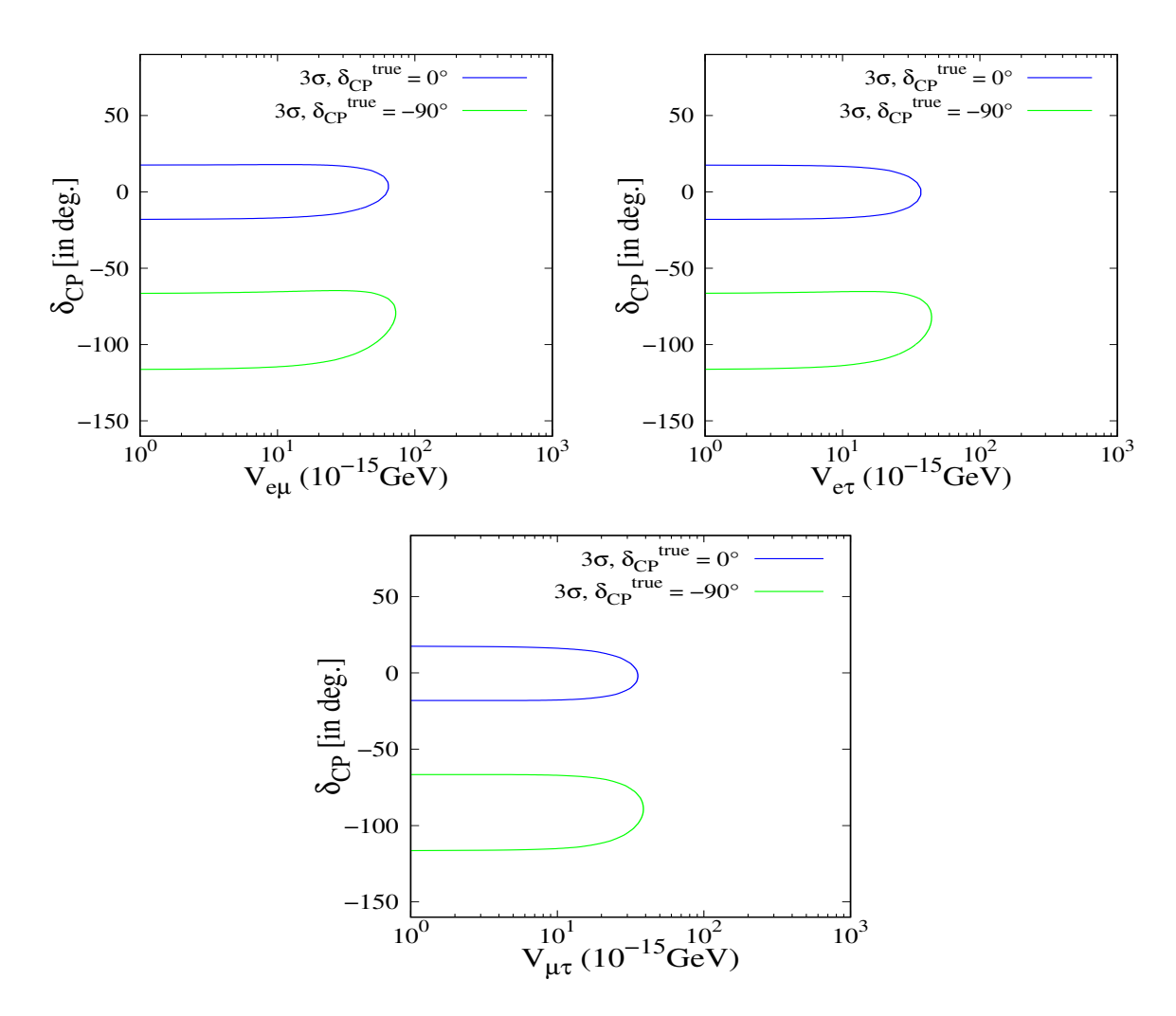


Figure 8. Effect of long-range interactions on the determination of $\delta_{\rm CP}$. In all the panels, two distinct true values for the leptonic CP-violating phase have been chosen, $\delta_{\rm CP}^{\rm true} = 0^{\circ}, -90^{\circ}$.

over the full range $[-180^{\circ}, 180^{\circ}]$ and compare this with $\delta_{\rm CP} = 0^{\circ}$ or 180° in the test. The same value of LRF potentials $V_{\alpha\beta}$ is considered in both true and test event spectra. The CPV-sensitivity plots are displayed in figure 9 in units of $\sqrt{\Delta\chi^2}$, where

$$\Delta \chi^2 = \chi^2(V_{\alpha\beta}, \text{CPV}) - \chi^2(V_{\alpha\beta}, \delta_{\text{CP}} = 0^\circ, 180^\circ).$$
 (6.1)

In this figure, the red curve represents the sensitivity in the standard oscillation scenario $(V_{\alpha\beta}=0)$. The dashed, dotted and dashdot curves are for the potentials $V_{e\mu}$, $V_{e\tau}$ and $V_{\mu\tau}$, respectively. The sensitivity curves plotted in blue colour correspond to the value of $V_{\alpha\beta}=5\times10^{-14}\,\mathrm{eV}$, which is comparable to the ESSnuSB constraints, while the curves in green are computed for the LRF potentials, $V_{\alpha\beta}=5\times10^{-13}\,\mathrm{eV}$, a much larger potential value than the ESSnuSB bounds. We notice that for small values of the new potentials, the ESSnuSB CP-violation sensitivity remains intact with some negligible impact on its sensitivity around $\delta_{\mathrm{CP}}=\pm90^{\circ}$. However, for large values of the LRF potentials, the $\Delta\chi^2$ changes and the positions of the sensitivity maxima are also slightly shifted. To understand

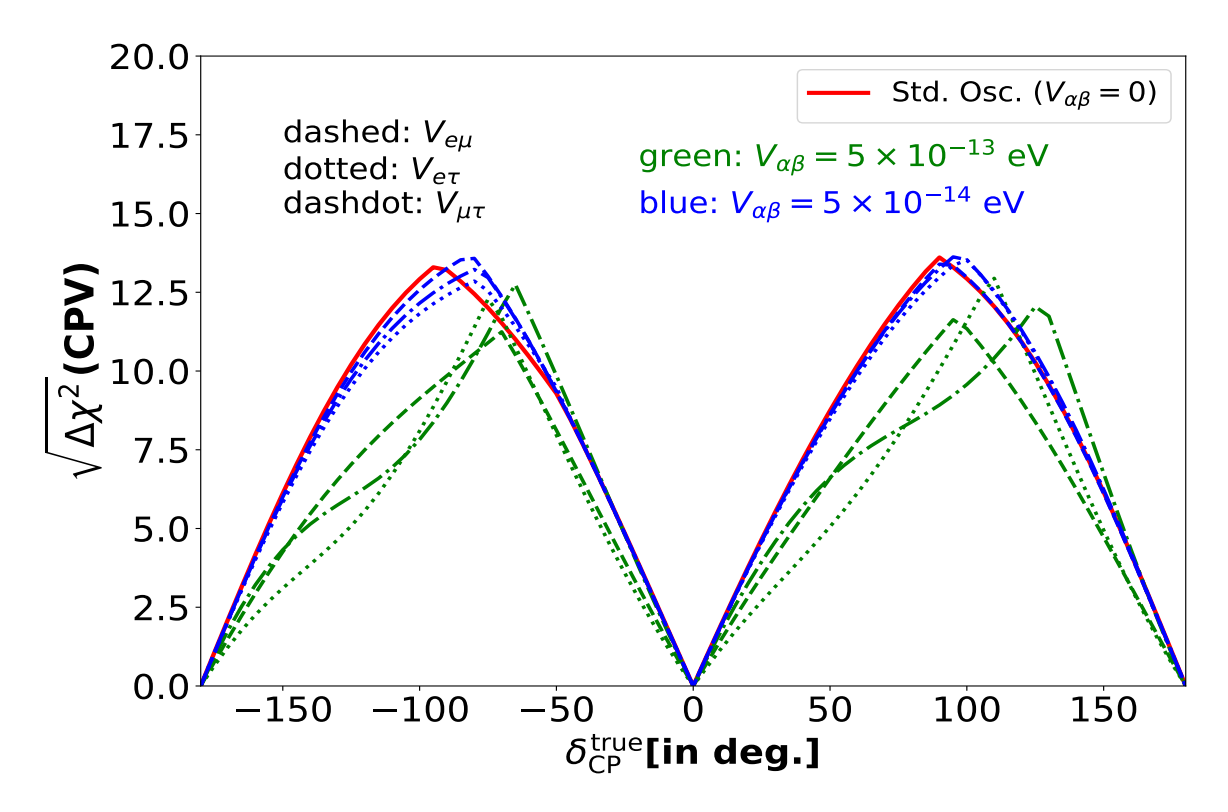


Figure 9. CP-violation sensitivity of ESSnuSB for different values of LRF potentials $V_{\alpha\beta}$ and symmetries. Here, both true and test hypotheses assume the presence of LRFs. Standard oscillation $(V_{\alpha\beta}=0)$ is shown by the solid red curve.

this in more detail, we compute the CPV sensitivity as a function of the LRF potentials, $V_{\alpha\beta}$. The results are displayed in figure 10 for two choices of $\delta_{\rm CP}$, i.e. $+90^{\circ}$ (solid curves) and -90° (dashed curves). We can observe that, for small values of $V_{\alpha\beta}$ ($\lesssim 10^{-14} \, {\rm eV}$), the $\delta_{\rm CP}$ sensitivity of ESSnuSB more or less does not change for all three cases of $V_{\alpha\beta}$. However, with increasing $V_{\alpha\beta}$, the sensitivity decreases, especially for the potential corresponding to the $L_e - L_{\tau}$ symmetry. The reason is that when $V_{\alpha\beta}$ are small, they appear as a correction to the standard probability and mildly affect the $\delta_{\rm CP}$ sensitivity, whereas, for large values of $V_{\alpha\beta}$, new resonances might appear, causing a significant drop in the CPV sensitivity of ESSnuSB.

7 CP precision of ESSnuSB in the presence of LRFs

In this section, we will try to understand the impact of LRF potentials on the uncertainty of $\delta_{\rm CP}$ measurement by the ESSnuSB experiment. Since the primary objective of ESSnuSB is to perform a precision measurement of $\delta_{\rm CP}$ in addition to discovering it (if next-generation LBL experiments fall short), it is imperative to see how new physics affects this capability of ESSnuSB. In refs. [9, 47], it has been shown that the optimal baseline of 360 km allows the ESSnuSB experiment to measure $\delta_{\rm CP}$ with a 1σ uncertainty of less than 7.5° for all possible values of $\delta_{\rm CP}$. Remarkably, the experiment achieves its best precision, $\Delta \delta_{\rm CP} = 5^{\circ}$, for CP-conserving values. Such a level of accuracy is unparalleled, as it surpasses the capabilities

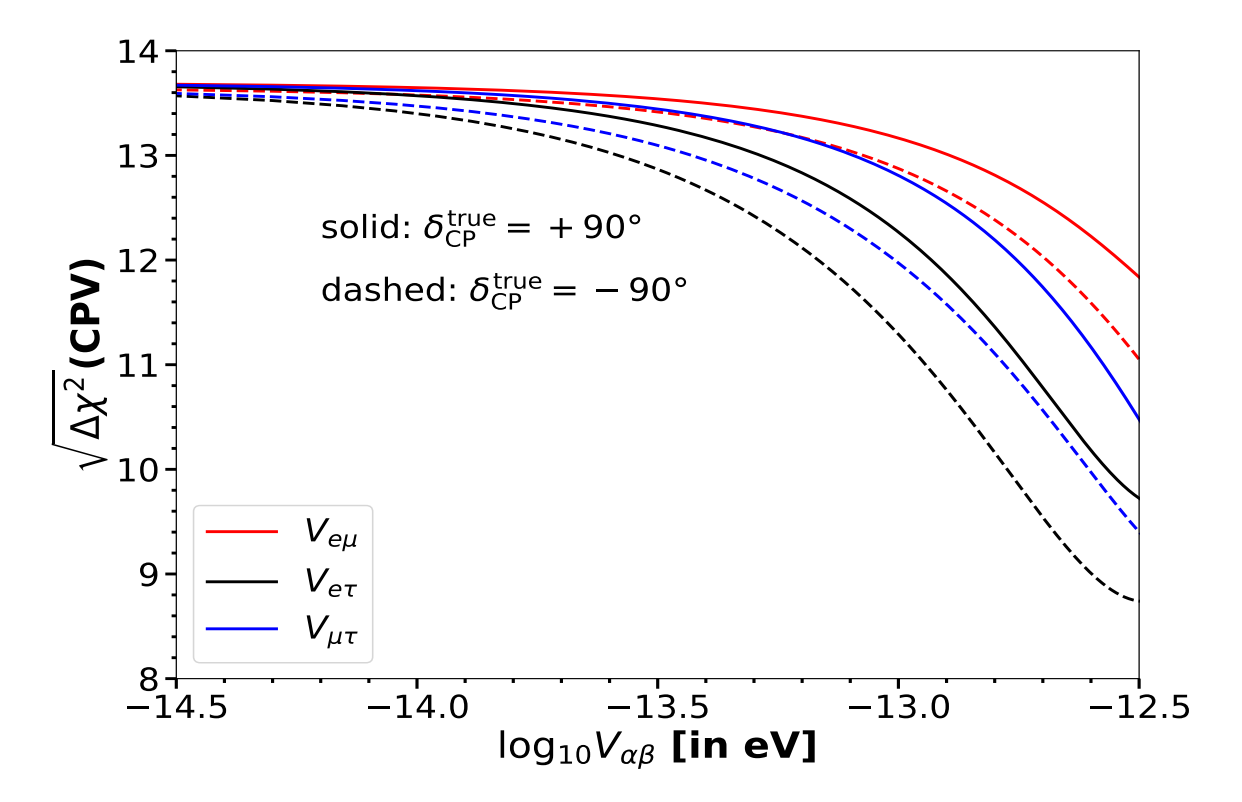


Figure 10. CP-violation sensitivity of ESSnuSB as a function of long-range potential $V_{\alpha\beta}$. The solid (dashed) curves correspond to the true value of $\delta_{\rm CP} = +90^{\circ}(-90^{\circ})$.

of next-generation LBL experiments, emphasizing the transformative potential of ESSnuSB in this area of research.

In figure 11, we present the projected 1σ uncertainty in the measurement of $\delta_{\rm CP}$ for two scenarios: the CP-conserving values ($\delta_{\rm CP}=0^\circ$ and 180° , shown in the left panel) and the maximally CP-violating values ($\delta_{\rm CP}=\pm90^\circ$, shown in the right panel), as functions of the LRF potentials, $V_{\alpha\beta}$. In both panels, solid, dashed and dashdot curves represent LRF potentials, namely, $V_{e\mu}$, $V_{e\tau}$ and $V_{\mu\tau}$, respectively. From figure 11 it is evident that the effects of LRF potentials on the $\delta_{\rm CP}$ precision of ESSnuSB are negligible. Even when the values of all three potentials are large enough (almost an order of magnitude larger than the ESSnuSB bounds), the effects of $V_{\alpha\beta}$ are not significant enough to meaningfully degrade the performance of ESSnuSB. Specifically, for the maximally CP-violating values ($\delta_{\rm CP}=\pm90^\circ$), illustrated in the right panel of figure 11, the experiment can achieve a robust precision of $\Delta\delta_{\rm CP}<7.5^\circ$, as long as $V_{\alpha\beta}$ remain below $2\times10^{-14}\,\rm eV$. For the CP-conserving values ($\delta_{\rm CP}=0^\circ$ and 180°), illustrated in the left panel of figure 11, the precision is even better, with $\Delta\delta_{\rm CP}\lesssim7^\circ$ across the entire range of LRF potentials, $V_{\alpha\beta}$.

These results highlight the resilience of ESSnuSB in maintaining high precision in δ_{CP} measurements, even in the presence of LRFs, further demonstrating its capability to probe CP violation with unprecedented accuracy.

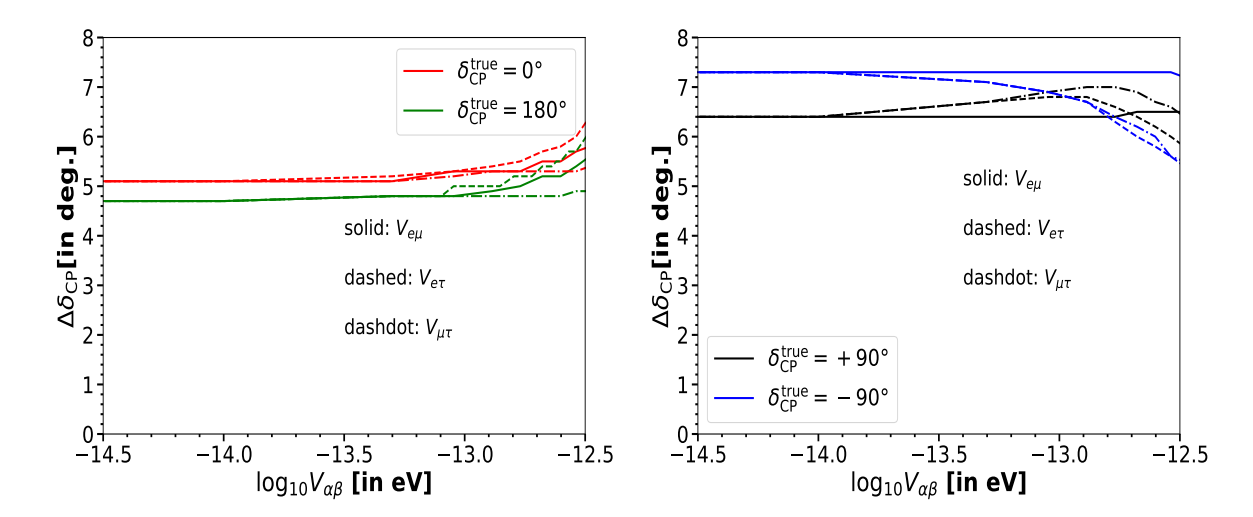


Figure 11. 1σ precision on the measurement of $\delta_{\rm CP}$ at ESSnuSB as a function of the LRF potential $V_{\alpha\beta}$, for three different choices of symmetries. The LRF potential $V_{\alpha\beta}$ is present in both true and test data. The left (right) plot corresponds to the true values of $\delta_{\rm CP} = 0^{\circ}$ and 180° ($\pm 90^{\circ}$).

8 Summary and conclusions

In this paper, we explored the capabilities of the ESSnuSB experiment to set bounds on the effects of LRFs in neutrino oscillations. In the presence of additional U(1) gauge symmetries in the particle physics Lagrangian, a new vector mediator Z' might be responsible for new interactions between SM particles. In the case of a very light mediator, such interactions might occur at very long distances and feebly interacting particles like neutrinos could provide valuable information about them. For instance, in neutrino oscillation experiments, LRFs modify matter effects in the neutrino oscillation probabilities introducing new terms in the Hamiltonian. We considered three different U(1) symmetries, namely $L_e - L_{\mu}$, $L_e - L_{\tau}$ and $L_{\mu} - L_{\tau}$. We demonstrated how the ESSnuSB setup could provide a good environment to search for LRFs. In particular, using nominal conditions (5% systematics), we observed that ESSnuSB could be able to set 90% C.L. limits on $V_{e\mu} < 2.99 \times 10^{-14} \,\mathrm{eV}, V_{e\tau} < 2.05 \times 10^{-14} \,\mathrm{eV}$ and $V_{\mu\tau} < 1.81 \times 10^{-14} \, \text{eV}$. The bounds on such parameters have been obtained by means of a standard χ^2 analysis performed using the GloBES software. Among the upcoming next-generation LBL experiments, only DUNE is expected to outperform ESSnuSB, while T2HK will set weaker limits [39, 62]. The ESSnuSB bounds might become comparable to the DUNE ones if systematic uncertainties in both the appearance and disappearance channels are reduced for the ESSnuSB experiment. We explored the correlations between the LRF parameters and the most unknown oscillation parameters, namely θ_{23} and δ_{CP} . We found that the octant degeneracy of θ_{23} is broken in the presence of LRFs when $\theta_{23}^{\text{true}} = 42.2^{\circ}$. We also could not observe any strong correlation between δ_{CP} and the LRF potentials $V_{\alpha\beta}$.

Finally, we addressed another crucial point in the context of the ESSnuSB experiment: the robustness of its most important measurement, namely the $\delta_{\rm CP}$ determination. We observed that, even in the presence of LRFs, both the CPV sensitivity and the $\delta_{\rm CP}$ precision remain unaltered except in the case of extremely large LRF potentials $(V_{\alpha\beta} \gg 10^{-13})$.

Acknowledgments

Funded by the European Union. Views and opinions expressed are however those of the author(s) only and do not necessarily reflect those of the European Union. Neither the European Union nor the granting authority can be held responsible for them.

We acknowledge further support provided by the following research funding agencies: Centre National de la Recherche Scientifique, France; Deutsche Forschungsgemeinschaft, Germany, Projektnummer 423761110; Ministry of Science and Education of Republic of Croatia grant No. KK.01.1.1.01.0001; the European Union's Horizon 2020 research and innovation programme under the Marie Skłodowska-Curie grant agreement No 860881-HIDDeN; the European Union NextGenerationEU, through the National Recovery and Resilience Plan of the Republic of Bulgaria, project No. BG-RRP-2.004-0008-C01; as well as support provided by the universities and laboratories to which the authors of this report are affiliated, see the author list on the first page.

A LRF induced by other U(1) symmetries

In ref. [50], other possibilities for the U(1) symmetries, which might generate new interactions modifying the neutrino oscillation probabilities, have been explored for the first time. In the context of neutrino oscillation, the different anomaly-free combinations of baryon number B and lepton numbers L_{α} [36, 54, 87–91] can only modify the diagonal entries of the matter potential part of the oscillation Hamiltonian (see table 3 for a list of the symmetries and ref. [50] for details). Thus, regardless of the specific combination of the charges of the particles under the specific symmetries, the only textures of the LRF matrix in the Hamiltonian not discussed in our previous analyses are [50]

$$V_{\alpha\beta} = \begin{cases} \operatorname{diag}(\pm V_{\text{LRF}}, 0, 0), & (\text{textures } A^{\pm}) \\ \operatorname{diag}(0, -V_{\text{LRF}}, 0), & (\text{texture } B) \\ \operatorname{diag}(0, 0, -V_{\text{LRF}}), & (\text{texture } C) \end{cases}$$
(A.1)

To quantitatively discuss the effects of the LRF mediated by the symmetries generating the $V_{\alpha\beta}$ matrices in the oscillation Hamiltonian, we show in figure 12 the $\stackrel{(-)}{\nu_{\mu}} \rightarrow \stackrel{(-)}{\nu_{e}}$ (panels a and c) and $\stackrel{(-)}{\nu_{\mu}} \rightarrow \stackrel{(-)}{\nu_{\mu}}$ (panels b and d) oscillation probabilities in the energy range interesting for ESSnuSB. In the appearance probability, the textures A^{+} and C have the same effect enhancing (reducing) the neutrino (antineutrino) probability at oscillation maximum by roughly the same amount. The A^{-} texture, on the other hand, has approximately the same but opposite effect of the A^{+} texture. The B texture does not significantly affect the oscillations. This behaviour also explains why the $L_{e}-L_{\tau}$ symmetry modifies the probabilities more than $L_{e}-L_{\mu}$ and $L_{\mu}-L_{\tau}$; indeed in this specific case, the effects of the A^{+} and C texture are summed, enhancing the probabilities more. The disappearance probabilities, on the other hand, are almost unaffected by the A^{\pm} textures and for the neutrino case, $P_{\mu\mu}$ is enhanced (reduced) at the minimum by the B (C) textures. The antineutrino disappearance probability exhibits opposite behaviour compared to the neutrino case when textures B and C are considered.

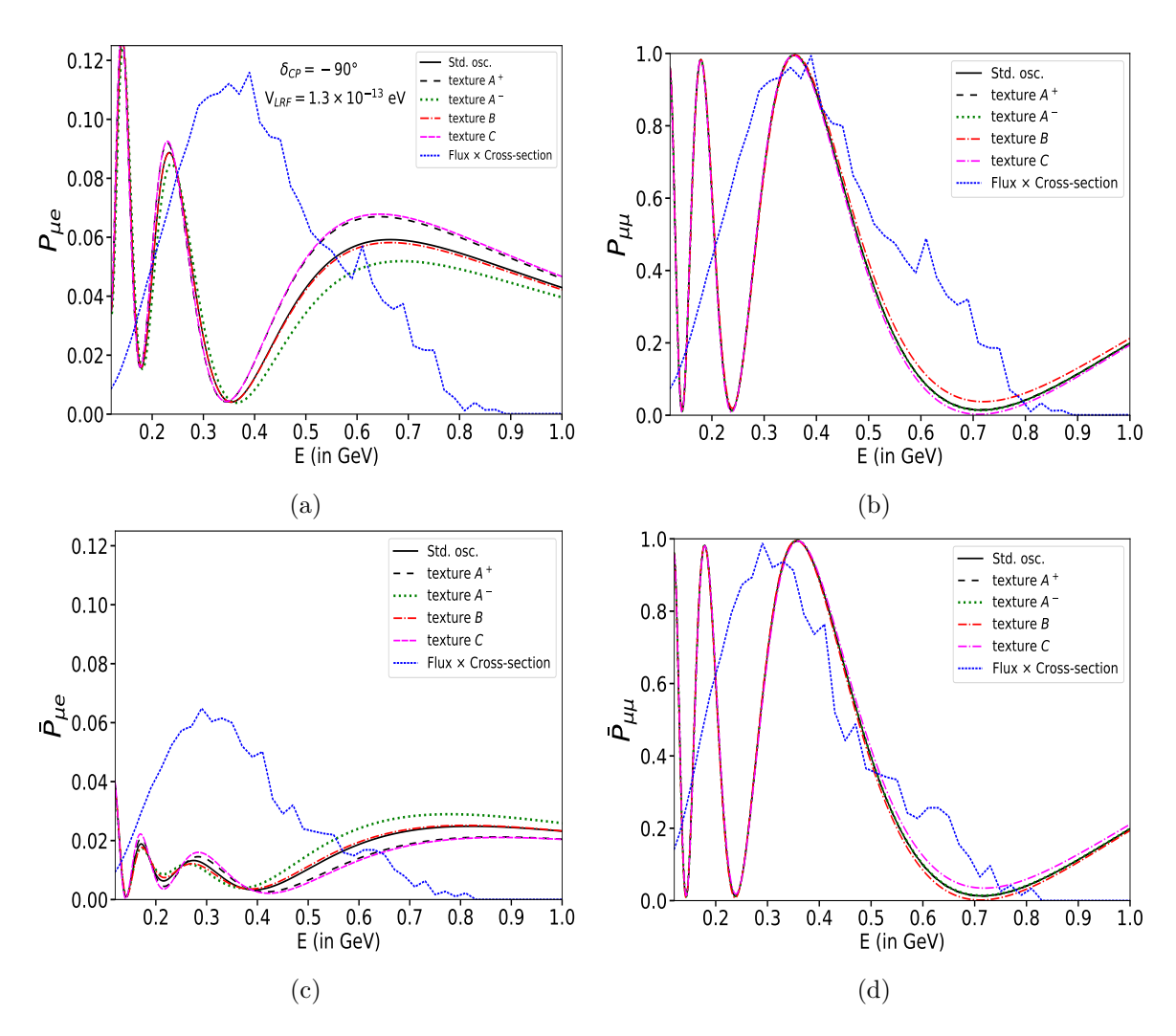


Figure 12. Appearance (left panel) and disappearance (right panel) neutrino (top panel) and antineutrino (bottom panel) oscillation probabilities as functions of neutrino energy in the presence of LRF potentials induced by other sorts of anomaly-free symmetries.

We finally study the sensitivity of the ESSnuSB experiment to the $V_{\rm LRF}$ parameters in the four studied cases in figure 13. We summarize in table 3 the 3σ bounds for the four textures obtained using the same procedure described in section 5 with 5% systematics. The bounds in these cases are, in general, less stringent than in the $L_{\alpha}-L_{\beta}$ symmetries cases. In particular, the texture C gives the tightest bound on $V_{\rm LRF}$, while the texture B is the looser. It is interesting to notice that since texture B does not affect significantly the appearance channel but only the disappearance one, the octant degeneracy causes a reduction of the 3σ sensitivity for $V_{\rm LRF}$.

Data Availability Statement. This article has no associated data or the data will not be deposited.

Code Availability Statement. This article has no associated code or the code will not be deposited.

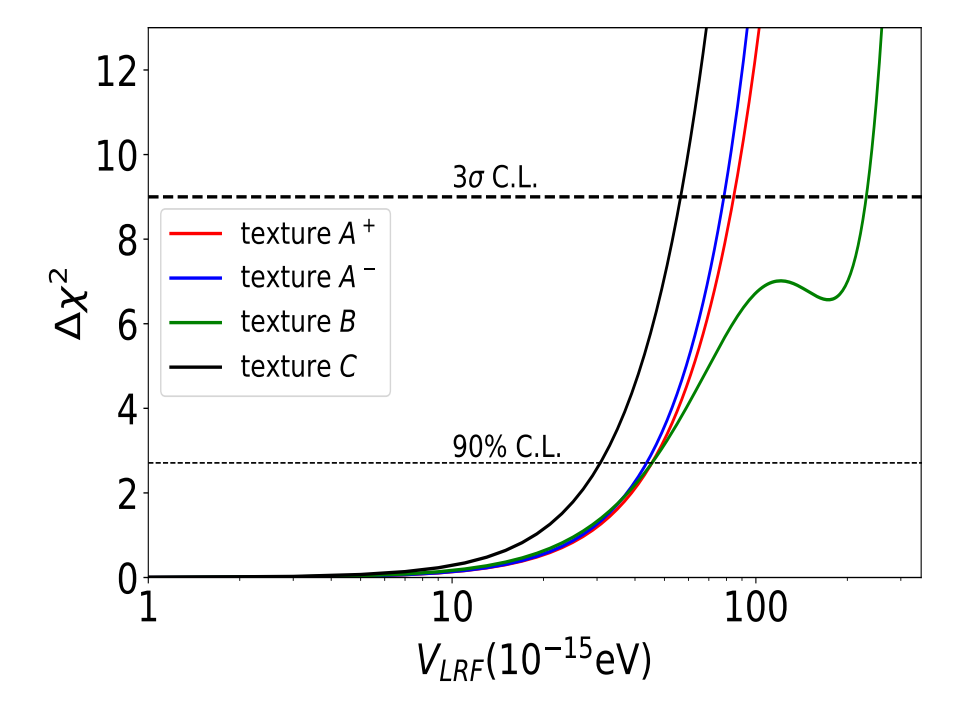


Figure 13. Sensitivity of ESSnuSB to constrain the LRF potentials induced by different U' symmetries mentioned in ref. [50]. In this case, we have used the standard 5% systematics of the ESSnuSB experiment.

LRF Potential Textures	$3\sigma \text{ C.L.}$ (×10 ⁻¹⁴) eV	90% C.L. $(\times 10^{-14}) \text{ eV}$	U(1) symmetries from ref. [50]
A^+	8.45	4.55	$B - 3L_e L - 3L_e B_y - \frac{3}{2}(L_{\mu} - L_{\tau}) L_e - \frac{1}{2}(L_{\mu} - L_{\tau})$
A^-	7.85	4.37	$L_e + 2L_{\mu} + 2L_{\tau}$ $B + L_{\mu} + L_{\tau}$
В	23.09	4.55	$B - 3L_{\mu}$ $L - 3L_{\mu}$
C	5.65	3.08	$B - 3L_{\tau}$ $L - 3L_{\tau}$

Table 3. Constraints on LRF potential $V_{\alpha\beta}$, considering other U(1) symmetries, using the ESSnuSB experiment for 5% systematics. These values are obtained from the plots displayed in figure 13. In the last column, we show the symmetries mentioned in ref. [50], where L is the lepton number, B is the baryon number and $B_y = B_1 - yB_2 - (3-y)B_3$ with B_i being the baryon numbers of the quark families and y an arbitrary constant.

Open Access. This article is distributed under the terms of the Creative Commons Attribution License (CC-BY4.0), which permits any use, distribution and reproduction in any medium, provided the original author(s) and source are credited.

References

- [1] SUPER-KAMIOKANDE collaboration, Evidence for oscillation of atmospheric neutrinos, Phys. Rev. Lett. 81 (1998) 1562 [hep-ex/9807003] [INSPIRE].
- [2] SNO collaboration, Direct evidence for neutrino flavor transformation from neutral current interactions in the Sudbury Neutrino Observatory, Phys. Rev. Lett. 89 (2002) 011301 [nucl-ex/0204008] [INSPIRE].
- [3] T. Kajita, Nobel Lecture: Discovery of atmospheric neutrino oscillations, Rev. Mod. Phys. 88 (2016) 030501 [INSPIRE].
- [4] A.B. McDonald, Nobel Lecture: The Sudbury Neutrino Observatory: Observation of flavor change for solar neutrinos, Rev. Mod. Phys. 88 (2016) 030502 [INSPIRE].
- [5] L. Wolfenstein, Neutrino Oscillations in Matter, Phys. Rev. D 17 (1978) 2369 [INSPIRE].
- [6] J. Kopp, M. Lindner, T. Ota and J. Sato, Non-standard neutrino interactions in reactor and superbeam experiments, Phys. Rev. D 77 (2008) 013007 [arXiv:0708.0152] [INSPIRE].
- [7] Y. Du et al., Non-standard interactions in SMEFT confronted with terrestrial neutrino experiments, JHEP 03 (2021) 019 [arXiv:2011.14292] [INSPIRE].
- [8] A. Gupta, D. Majumdar and S. Prakash, Neutrino oscillation measurements with KamLAND and JUNO in the presence of scalar NSI, arXiv:2306.07343 [INSPIRE].
- [9] ESSNUSB collaboration, Study of nonstandard interactions mediated by a scalar field at the ESSnuSB experiment, Phys. Rev. D 109 (2024) 115010 [arXiv:2310.10749] [INSPIRE].
- [10] P.B. Denton, A. Giarnetti and D. Meloni, Solar neutrinos and the strongest oscillation constraints on scalar NSI, JHEP 01 (2025) 097 [arXiv:2409.15411] [INSPIRE].
- [11] T. Ohlsson, Status of non-standard neutrino interactions, Rept. Prog. Phys. **76** (2013) 044201 [arXiv:1209.2710] [INSPIRE].
- [12] O.G. Miranda and H. Nunokawa, Non standard neutrino interactions: current status and future prospects, New J. Phys. 17 (2015) 095002 [arXiv:1505.06254] [INSPIRE].
- [13] Y. Farzan and M. Tortola, Neutrino oscillations and Non-Standard Interactions, Front. in Phys.
 6 (2018) 10 [arXiv:1710.09360] [INSPIRE].
- [14] P.S. Bhupal Dev et al., Neutrino Non-Standard Interactions: A Status Report, SciPost Phys. Proc. 2 (2019) 001 [arXiv:1907.00991] [INSPIRE].
- [15] K. Huitu, T.J. Kärkkäinen, J. Maalampi and S. Vihonen, Constraining the nonstandard interaction parameters in long baseline neutrino experiments, Phys. Rev. D 93 (2016) 053016 [arXiv:1601.07730] [INSPIRE].
- [16] M.E. Chaves, P.C. de Holanda and O.L.G. Peres, Testing non-standard neutrino interactions in (anti)-electron neutrino disappearance experiments, JHEP 03 (2023) 180 [arXiv:2106.15725] [INSPIRE].
- [17] X.G. He, G.C. Joshi, H. Lew and R.R. Volkas, New Z-prime Phenomenology, Phys. Rev. D 43 (1991) 22 [INSPIRE].

- [18] R. Foot, New Physics From Electric Charge Quantization?, Mod. Phys. Lett. A 6 (1991) 527 [INSPIRE].
- [19] X.-G. He, G.C. Joshi, H. Lew and R.R. Volkas, Simplest Z-prime model, Phys. Rev. D 44 (1991) 2118 [INSPIRE].
- [20] R. Foot, X.G. He, H. Lew and R.R. Volkas, Model for a light Z-prime boson, Phys. Rev. D 50 (1994) 4571 [hep-ph/9401250] [INSPIRE].
- [21] A.D. Dolgov, Long range forces in the universe, Phys. Rept. 320 (1999) 1 [INSPIRE].
- [22] A.Y. Smirnov and X.-J. Xu, Wolfenstein potentials for neutrinos induced by ultra-light mediators, JHEP 12 (2019) 046 [arXiv:1909.07505] [INSPIRE].
- [23] B. Pontecorvo, Neutrino Experiments and the Problem of Conservation of Leptonic Charge, Zh. Eksp. Teor. Fiz. 53 (1967) 1717 [INSPIRE].
- [24] V.N. Gribov and B. Pontecorvo, Neutrino astronomy and lepton charge, Phys. Lett. B 28 (1969) 493 [INSPIRE].
- [25] V. Cirigliano, B. Grinstein, G. Isidori and M.B. Wise, *Minimal flavor violation in the lepton sector*, *Nucl. Phys. B* **728** (2005) 121 [hep-ph/0507001] [INSPIRE].
- [26] G. Altarelli and F. Feruglio, Discrete Flavor Symmetries and Models of Neutrino Mixing, Rev. Mod. Phys. 82 (2010) 2701 [arXiv:1002.0211] [INSPIRE].
- [27] K. Asai, K. Hamaguchi and N. Nagata, Predictions for the neutrino parameters in the minimal gauged $U(1)_{L_u-L_\tau}$ model, Eur. Phys. J. C 77 (2017) 763 [arXiv:1705.00419] [INSPIRE].
- [28] K. Asai et al., Minimal Gauged $U(1)_{L_{\alpha}-L_{\beta}}$ Models Driven into a Corner, Phys. Rev. D 99 (2019) 055029 [arXiv:1811.07571] [INSPIRE].
- [29] Y. Lou and T. Nomura, Neutrino observables in gauged $U(1)_{L_{\alpha}-L_{\beta}}$ models with two Higgs doublet and one singlet scalars, Chin. Phys. C 49 (2025) 053003 [arXiv:2406.01030] [INSPIRE].
- [30] J.A. Grifols and E. Masso, Neutrino oscillations in the sun probe long range leptonic forces, Phys. Lett. B 579 (2004) 123 [hep-ph/0311141] [INSPIRE].
- [31] A. Bandyopadhyay, A. Dighe and A.S. Joshipura, Constraints on flavor-dependent long range forces from solar neutrinos and KamLAND, Phys. Rev. D 75 (2007) 093005 [hep-ph/0610263] [INSPIRE].
- [32] M.C. Gonzalez-Garcia, P.C. de Holanda, E. Masso and R. Zukanovich Funchal, Probing long-range leptonic forces with solar and reactor neutrinos, JCAP 01 (2007) 005 [hep-ph/0609094] [INSPIRE].
- [33] A.S. Joshipura and S. Mohanty, Constraints on flavor dependent long range forces from atmospheric neutrino observations at super-Kamiokande, Phys. Lett. B **584** (2004) 103 [hep-ph/0310210] [INSPIRE].
- [34] M. Bustamante and S.K. Agarwalla, Universe's Worth of Electrons to Probe Long-Range Interactions of High-Energy Astrophysical Neutrinos, Phys. Rev. Lett. 122 (2019) 061103 [arXiv:1808.02042] [INSPIRE].
- [35] S.K. Agarwalla, M. Bustamante, S. Das and A. Narang, Present and future constraints on flavor-dependent long-range interactions of high-energy astrophysical neutrinos, JHEP 08 (2023) 113 [arXiv:2305.03675] [INSPIRE].
- [36] P. Coloma, M.C. Gonzalez-Garcia and M. Maltoni, Neutrino oscillation constraints on U(1)' models: from non-standard interactions to long-range forces, JHEP 01 (2021) 114 [Erratum ibid. 11 (2022) 115] [arXiv:2009.14220] [INSPIRE].

- [37] S.S. Chatterjee, A. Dasgupta and S.K. Agarwalla, Exploring Flavor-Dependent Long-Range Forces in Long-Baseline Neutrino Oscillation Experiments, JHEP 12 (2015) 167 [arXiv:1509.03517] [INSPIRE].
- [38] A. Khatun, T. Thakore and S. Kumar Agarwalla, Can INO be Sensitive to Flavor-Dependent Long-Range Forces?, JHEP 04 (2018) 023 [arXiv:1801.00949] [INSPIRE].
- [39] M. Singh, M. Bustamante and S.K. Agarwalla, Flavor-dependent long-range neutrino interactions in DUNE & T2HK: alone they constrain, together they discover, JHEP 08 (2023) 101 [arXiv:2305.05184] [INSPIRE].
- [40] P. Mishra et al., Study of long range force in P2SO and T2HKK, JHEP **09** (2024) 100 [arXiv:2402.19178] [INSPIRE].
- [41] T2K collaboration, Combined Analysis of Neutrino and Antineutrino Oscillations at T2K, Phys. Rev. Lett. 118 (2017) 151801 [arXiv:1701.00432] [INSPIRE].
- [42] T2K collaboration, Constraint on the matter-antimatter symmetry-violating phase in neutrino oscillations, Nature **580** (2020) 339 [Erratum ibid. **583** (2020) E16] [arXiv:1910.03887] [INSPIRE].
- [43] NOvA collaboration, First Measurement of Neutrino Oscillation Parameters using Neutrinos and Antineutrinos by NOvA, Phys. Rev. Lett. 123 (2019) 151803 [arXiv:1906.04907] [INSPIRE].
- [44] DUNE collaboration, Long-baseline neutrino oscillation physics potential of the DUNE experiment, Eur. Phys. J. C 80 (2020) 978 [arXiv:2006.16043] [INSPIRE].
- [45] ESSNUSB collaboration, Updated physics performance of the ESSnuSB experiment: ESSnuSB collaboration, Eur. Phys. J. C 81 (2021) 1130 [arXiv:2107.07585] [INSPIRE].
- [46] H. Abele et al., Particle Physics at the European Spallation Source, Phys. Rept. 1023 (2023) 1 [arXiv:2211.10396] [INSPIRE].
- [47] A. Alekou et al., The European Spallation Source neutrino super-beam conceptual design report, Eur. Phys. J. ST 231 (2022) 3779 [arXiv:2206.01208] [INSPIRE].
- [48] ESSNUSB collaboration, The ESSnuSB Design Study: Overview and Future Prospects, Universe 9 (2023) 347 [arXiv:2303.17356] [INSPIRE].
- [49] ESSNUSB collaboration, Search for Leptonic CP Violation with the ESSnuSBplus Project, LHEP 2024 (2024) 517 [INSPIRE].
- [50] S.K. Agarwalla, M. Bustamante, M. Singh and P. Swain, A plethora of long-range neutrino interactions probed by DUNE and T2HK, JHEP 09 (2024) 055 [arXiv:2404.02775] [INSPIRE].
- [51] S. Choubey, S. Khan, M. Merchand and S. Vihonen, Constraining dark matter from strong phase transitions in a $U(1)_{L_{\mu}-L_{\tau}}$ model: implications for neutrino masses and muon g-2, JHEP 10 (2024) 186 [arXiv:2406.16460] [INSPIRE].
- [52] M. Ibe, S. Shirai and K. Watanabe, Global Neutrino Constraints on the Minimal $U(1)_{L_{\mu}-L_{\tau}}$ Model, Phys. Rev. D 111 (2025) 095034 [arXiv:2503.01399] [INSPIRE].
- [53] K.S. Babu, C.F. Kolda and J. March-Russell, Implications of generalized Z–Z-prime mixing, Phys. Rev. D 57 (1998) 6788 [hep-ph/9710441] [INSPIRE].
- [54] A.S. Joshipura, N. Mahajan and K.M. Patel, Generalised μ - τ symmetries and calculable gauge kinetic and mass mixing in U(1) $_{L_{\mu}-L_{\tau}}$ models, JHEP **03** (2020) 001 [arXiv:1909.02331] [INSPIRE].
- [55] B. Holdom, Two U(1)'s and Epsilon Charge Shifts, Phys. Lett. B 166 (1986) 196 [INSPIRE].

- [56] A. Ghoshal, A. Giarnetti and D. Meloni, Neutrino Invisible Decay at DUNE: a multi-channel analysis, J. Phys. G 48 (2021) 055004 [arXiv:2003.09012] [INSPIRE].
- [57] J. Gehrlein, P.A.N. Machado and J.P. Pinheiro, Constraining non-standard neutrino interactions with neutral current events at long-baseline oscillation experiments, JHEP 05 (2025) 065 [arXiv:2412.08712] [INSPIRE].
- [58] P.B. Denton, A. Giarnetti and D. Meloni, How to identify different new neutrino oscillation physics scenarios at DUNE, JHEP 02 (2023) 210 [arXiv:2210.00109] [INSPIRE].
- [59] S.K. Agarwalla, S. Das, A. Giarnetti and D. Meloni, Model-independent constraints on non-unitary neutrino mixing from high-precision long-baseline experiments, JHEP 07 (2022) 121 [arXiv:2111.00329] [INSPIRE].
- [60] P. Coloma, D.V. Forero and S.J. Parke, *DUNE Sensitivities to the Mixing between Sterile and Tau Neutrinos*, *JHEP* **07** (2018) 079 [arXiv:1707.05348] [INSPIRE].
- [61] A. Giarnetti and D. Meloni, New Sources of Leptonic CP Violation at the DUNE Neutrino Experiment, Universe 7 (2021) 240 [arXiv:2106.00030] [INSPIRE].
- [62] A. Giarnetti, S. Marciano and D. Meloni, Exploring New Physics with Deep Underground Neutrino Experiment High-Energy Flux: The Case of Lorentz Invariance Violation, Large Extra Dimensions and Long-Range Forces, Universe 10 (2024) 357 [arXiv:2407.17247] [INSPIRE].
- [63] J.M. Berryman et al., Large, Extra Dimensions at the Deep Underground Neutrino Experiment, Phys. Rev. D 94 (2016) 033006 [arXiv:1603.00018] [INSPIRE].
- [64] M.B. Wise and Y. Zhang, Lepton Flavorful Fifth Force and Depth-dependent Neutrino Matter Interactions, JHEP 06 (2018) 053 [arXiv:1803.00591] [INSPIRE].
- [65] J. Heeck and W. Rodejohann, Gauged $L_{\mu} L_{\tau}$ and different Muon Neutrino and Anti-Neutrino Oscillations: MINOS and beyond, J. Phys. G 38 (2011) 085005 [arXiv:1007.2655] [INSPIRE].
- [66] S.K. Agarwalla, S. Das, M. Masud and P. Swain, Evolution of neutrino mass-mixing parameters in matter with non-standard interactions, JHEP 11 (2021) 094 [arXiv:2103.13431] [INSPIRE].
- [67] T. Kikuchi, H. Minakata and S. Uchinami, Perturbation Theory of Neutrino Oscillation with Nonstandard Neutrino Interactions, JHEP 03 (2009) 114 [arXiv:0809.3312] [INSPIRE].
- [68] P. Huber, M. Lindner and W. Winter, Simulation of long-baseline neutrino oscillation experiments with GLoBES (General Long Baseline Experiment Simulator), Comput. Phys. Commun. 167 (2005) 195 [hep-ph/0407333] [INSPIRE].
- [69] P. Huber et al., New features in the simulation of neutrino oscillation experiments with GLoBES 3.0: General Long Baseline Experiment Simulator, Comput. Phys. Commun. 177 (2007) 432 [hep-ph/0701187] [INSPIRE].
- [70] ESSNUSB collaboration, Decoherence in neutrino oscillation at the ESSnuSB experiment, JHEP 08 (2024) 063 [arXiv:2404.17559] [INSPIRE].
- [71] I. Esteban et al., The fate of hints: updated global analysis of three-flavor neutrino oscillations, JHEP 09 (2020) 178 [arXiv:2007.14792] [INSPIRE].
- [72] NuFIT 5.2, (2022), http://www.nu-fit.org/.
- [73] F. Capozzi et al., Global constraints on absolute neutrino masses and their ordering, Phys. Rev. D 95 (2017) 096014 [Addendum ibid. 101 (2020) 116013] [arXiv:2003.08511] [INSPIRE].
- [74] I. Esteban et al., Global analysis of three-flavour neutrino oscillations: synergies and tensions in the determination of θ_{23} , δ_{CP} , and the mass ordering, JHEP **01** (2019) 106 [arXiv:1811.05487] [INSPIRE].

- [75] P.F. de Salas et al., 2020 global reassessment of the neutrino oscillation picture, JHEP **02** (2021) 071 [arXiv:2006.11237] [INSPIRE].
- [76] F. Capozzi et al., Unfinished fabric of the three neutrino paradigm, Phys. Rev. D 104 (2021) 083031 [arXiv:2107.00532] [INSPIRE].
- [77] M.C. Gonzalez-Garcia, M. Maltoni and T. Schwetz, NuFIT: Three-Flavour Global Analyses of Neutrino Oscillation Experiments, Universe 7 (2021) 459 [arXiv:2111.03086] [INSPIRE].
- [78] J.-Q. Jiang et al., Neutrino cosmology after DESI: tightest mass upper limits, preference for the normal ordering, and tension with terrestrial observations, JCAP 01 (2025) 153 [arXiv:2407.18047] [INSPIRE].
- [79] P. Huber, M. Lindner and W. Winter, Superbeams versus neutrino factories, Nucl. Phys. B 645 (2002) 3 [hep-ph/0204352] [INSPIRE].
- [80] G.L. Fogli et al., Getting the most from the statistical analysis of solar neutrino oscillations, Phys. Rev. D 66 (2002) 053010 [hep-ph/0206162] [INSPIRE].
- [81] S.S. Wilks, The Large-Sample Distribution of the Likelihood Ratio for Testing Composite Hypotheses, Annals Math. Statist. 9 (1938) 60 [INSPIRE].
- [82] W. Dehnen and J. Binney, Mass models of the Milky Way, Mon. Not. Roy. Astron. Soc. 294 (1998) 429 [astro-ph/9612059] [INSPIRE].
- [83] M.J. Miller and J.N. Bregman, The Structure of the Milky Way's Hot Gas Halo, Astrophys. J. 770 (2013) 118 [arXiv:1305.2430] [INSPIRE].
- [84] M. Baryakhtar, R. Lasenby and M. Teo, Black Hole Superradiance Signatures of Ultralight Vectors, Phys. Rev. D 96 (2017) 035019 [arXiv:1704.05081] [INSPIRE].
- [85] N. Arkani-Hamed, L. Motl, A. Nicolis and C. Vafa, The string landscape, black holes and gravity as the weakest force, JHEP 06 (2007) 060 [hep-th/0601001] [INSPIRE].
- [86] S.K. Agarwalla et al., Enhancing sensitivity to leptonic CP violation using complementarity among DUNE, T2HK, and T2HKK, Eur. Phys. J. C 83 (2023) 694 [arXiv:2211.10620] [INSPIRE].
- [87] H. Davoudiasl, H.-S. Lee and W.J. Marciano, Long-Range Lepton Flavor Interactions and Neutrino Oscillations, Phys. Rev. D 84 (2011) 013009 [arXiv:1102.5352] [INSPIRE].
- [88] T. Araki, J. Heeck and J. Kubo, Vanishing Minors in the Neutrino Mass Matrix from Abelian Gauge Symmetries, JHEP 07 (2012) 083 [arXiv:1203.4951] [INSPIRE].
- [89] L.M.G. de la Vega, L.J. Flores, N. Nath and E. Peinado, Complementarity between dark matter direct searches and CEνNS experiments in U(1)' models, JHEP 09 (2021) 146 [arXiv:2107.04037] [INSPIRE].
- [90] Y. Farzan and J. Heeck, Neutrinophilic nonstandard interactions, Phys. Rev. D 94 (2016) 053010 [arXiv:1607.07616] [INSPIRE].
- [91] Y. Almumin et al., Neutrino Flavor Model Building and the Origins of Flavor and CP Violation, Universe 9 (2023) 512 [arXiv:2204.08668] [INSPIRE].

The ESSnuSB collaboration

- J. Aguilar¹, M. Anastasopoulos², D. Barčot³, E. Baussan⁴, A.K. Bhattacharyya², A. Bignami²,
- M. Blennow^{5,6}, M. Bogomilov⁷, B. Bolling², E. Bouquerel⁴, F. Bramati⁸, A. Branca⁸, G. Brunetti⁸,
- I. Bustinduy¹, C.J. Carlile⁹, J. Cederkall⁹, T.W. Choi¹⁰, S. Choubey^{5,6}, P. Christiansen⁹,
- M. Collins^{2,11}, E. Cristaldo Morales⁸, P. Cupiał¹², D. D'Ago¹³, H. Danared², J.P.A.M. de André⁴,
- M. Dracos⁴, I. Efthymiopoulos¹⁴, T. Ekelöf¹⁰, M. Eshraqi², G. Fanourakis¹⁵, A. Farricker¹⁶,
- E. Fasoula^{17,18}, T. Fukuda¹⁹, N. Gazis², Th. Geralis¹⁵, M. Ghosh^{3,*}, A. Giarnetti^{20,*},
- G. Gokbulut^{21,22}, A. Gupta⁶^{23,24,*}, C. Hagner²⁵, L. Halić³, M. Hooft²², K.E. Iversen⁹,
- N. Jachowicz²², M. Jakkapu³, M. Jenssen², R. Johansson², E. Kasimi¹⁷, A. Kayis Topaksu²¹,
- B. Kildetoft², B. Kliček³, K. Kordas^{17,18}, B. Kovač³, A. Leisos²⁶, M. Lindroos^{2,9,†}, A. Longhin²⁷,
- C. Maiano², D. Majumdar²⁸, S. Marangoni⁸, S. Marciano²⁰, J.G. Marcos²², C. Marrelli¹⁴,
- D. Meloni [©] ^{20,*}, M. Mezzetto ¹³, N. Milas ², J.L. Muñoz ¹, K. Niewczas ²², M. Oglakci ²¹,
- T. Ohlsson 5,6, M. Olvegård, M. Pari²⁴, D. Patrzalek, G. Petkov, Ch. Petridou^{17,18}, P. Poussot,
- A Psallidas¹⁵, F. Pupilli¹³, D. Saiang²⁹, D. Sampsonidis^{17,18}, A. Scanu⁸, C. Schwab⁴, F. Sordo¹,
- G. Stavropoulos¹⁵, M. Stipčević³, R. Tarkeshian², F. Terranova⁸, T. Tolba²⁵, E. Trachanas²,
- R. Tsenov⁷, A. Tsirigotis²⁶, S.E. Tzamarias¹⁷, M. Vanderpoorten²², G. Vankova-Kirilova⁷,
- N. Vassilopoulos³⁰, S. Vihonen^{5,6}, J. Wurtz⁴, V. Zeter⁴, O. Zormpa¹⁵
 - ¹ Consorcio ESS-bilbao, Parque Científico y Tecnológico de Bizkaia, Laida Bidea, Edificio 207-B, 48160 Derio, Bizkaia, Spain
 - ² European Spallation Source, Box 176, SE-221 00 Lund, Sweden
 - ³ Center of Excellence for Advanced Materials and Sensing Devices, Ruđer Bošković Institute, 10000 Zagreb, Croatia
 - ⁴ IPHC. Université de Strasboura. CNRS/IN2P3. Strasbourg, France
 - Department of Physics, School of Engineering Sciences, KTH Royal Institute of Technology, Roslagstullsbacken 21, 106 91 Stockholm, Sweden
 - ⁶ The Oskar Klein Centre, AlbaNova University Center, Roslagstullsbacken 21, 106 91 Stockholm, Sweden
 - ⁷ Faculty of Physics, Sofia University St. Kliment Ohridski, 1164 Sofia, Bulgaria
 - ⁸ University of Milano-Bicocca and INFN Sez. di Milano-Bicocca, 20126 Milano, Italy
 - ⁹ Department of Physics, Lund University,
 - P.O Box 118, 221 00 Lund, Sweden
 - ¹⁰ Department of Physics and Astronomy, FREIA Division, Uppsala University, P.O. Box 516, 751 20 Uppsala, Sweden
 - ¹¹ Faculty of Engineering, Lund University, P.O Box 118, 221 00 Lund, Sweden
 - 12 AGH University of Krakow,
 - al. A. Mickiewicza 30, 30-059 Krakow, Poland
 - ¹³ INFN Sez. di Padova, Padova, Italy
- ¹⁴ CERN, 1211 Geneva 23, Switzerland
- ¹⁵ Institute of Nuclear and Particle Physics, NCSR Demokritos, Neapoleos 27, 15341 Agia Paraskevi, Greece
- ¹⁶ Cockroft Institute (A36), Liverpool University, Warrington WA4 4AD, U.K.
- ¹⁷ Department of Physics, Aristotle University of Thessaloniki, Thessaloniki, Greece

- 18 Center for Interdisciplinary Research and Innovation (CIRI-AUTH), Thessaloniki, Greece
- ¹⁹ Institute for Advanced Research, Nagoya University, Nagoya 464–8601, Japan
- ²⁰ Dipartimento di Matematica e Fisica, Università di Roma Tre, Via della Vasca Navale 84, 00146 Rome, Italy
- ²¹ Faculty of Science and Letters, Department of Physics, University of Cukurova, 01330 Adana, Turkey
- ²² Department of Physics and Astronomy, Ghent University, Proeftuinstraat 86, B-9000 Ghent, Belgium
- ²³ Theory Division, Saha Institute of Nuclear Physics, 1/AF, Bidhannagar, Kolkata 700064, India
- ²⁴ Homi Bhabha National Institute, Anushakti Nagar, Mumbai 400094, India
- ²⁵ Institute for Experimental Physics, Hamburg University, 22761 Hamburg, Germany
- ²⁶ Physics Laboratory, School of Science and Technology, Hellenic Open University, 26335, Patras, Greece
- ²⁷ Department of Physics and Astronomy "G. Galilei", University of Padova and INFN Sezione di Padova, Padova, Italy
- ²⁸ Department of Physics, Ramakrishna Mission Vivekananda Educational and Research Institute, Belur Math, Howrah, West Bengal 711202, India
- ²⁹ Department of Civil, Environmental and Natural Resources Engineering, Luleå University of Technology, SE-971 87 Lulea, Sweden
- ³⁰ Institute of High Energy Physics (IHEP) Dongguan Campus, Chinese Academy of Sciences (CAS), Guangdong 523803, China
- st Corresponding author
- † Deceased.